Article

Immunity

Calcitonin Gene-Related Peptide Negatively Regulates Alarmin-Driven Type 2 Innate Lymphoid Cell Responses

Graphical Abstract

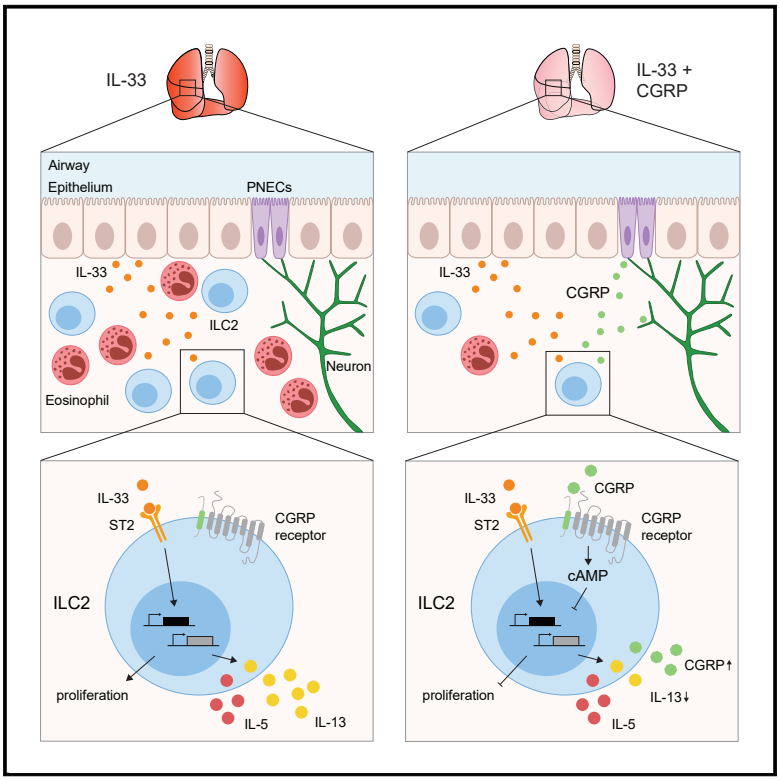

Highlights

- ILC2s express the neuropeptide CGRP and its receptor
- CGRP inhibits type 2 cytokine production and proliferation of activated ILC2s
- Treatment with CGRP negatively regulates IL-33-induced airway inflammation
- CGRP receptor-deficient mice show increased ILC2 responses to alarmins

Authors

Antonia Wallrapp, Patrick R. Burkett, Samantha J. Riesenfeld, ..., Bruce D. Levy, Aviv Regev, Vijay K. Kuchroo

Correspondence

aregev@broadinstitute.org (A.R.), vkuchroo@evergrande.hms.harvard.edu (V.K.K.)

In Brief

Cross-talk between neurons and ILC2s regulates tissue inflammation. Here, Wallrapp et al. show that the neuropeptide CGRP negatively regulates ILC2 responses to alarmins and inhibits airway inflammation *in vivo*. Mice lacking the CGRP receptor have exacerbated responses to alarmins, indicating this is an important pathway that controls type 2 inflammation.

Wallrapp et al., 2019, Immunity *51*, 709–723
October 15, 2019
https://doi.org/10.1016/j.immuni.2019.09.005

CellPress

Immunity
Article

Calcitonin Gene-Related Peptide Negatively Regulates Alarmin-Driven Type 2 Innate Lymphoid Cell Responses

Antonia Wallrapp,[1,9] Patrick R. Burkett,[1,2,9] Samantha J. Riesenfeld,[3,9] Se-Jin Kim,[1,2] Elena Christian,[1,3] Raja-Elie E. Abdulnour,[2] Pratiksha I. Thakore,[3] Alexandra Schnell,[1] Conner Lambden,[1,3] Rebecca H. Herbst,[3] Pavana Khan,[2] Kazutake Tsujikawa,[4] Ramnik J. Xavier,[5,6] Isaac M. Chiu,[7] Bruce D. Levy,[2] Aviv Regev,[3,8,*] and Vijay K. Kuchroo[1,3,10,*]

[1]Evergrande Center for Immunologic Diseases, Harvard Medical School and Brigham and Women's Hospital, Boston, MA 02115, USA
[2]Division of Pulmonary and Critical Care Medicine, Department of Medicine, Brigham and Women's Hospital, Boston, MA 02115, USA
[3]Klarman Cell Observatory, Broad Institute of MIT and Harvard, Cambridge, MA 02142, USA
[4]Laboratory of Molecular and Cellular Physiology, Graduate School of Pharmaceutical Sciences, Osaka University, Osaka, 565-0871, Japan
[5]Broad Institute of MIT and Harvard, Cambridge, MA 02142, USA
[6]Department of Molecular Biology, Massachusetts General Hospital, Boston, MA 02114, USA
[7]Department of Immunology, Harvard Medical School, Boston, MA 02115, USA
[8]Howard Hughes Medical Institute and Koch Institute for Integrative Cancer Research, Department of Biology, Massachusetts Institute of Technology, Cambridge, MA 02142, USA
[9]These authors contributed equally
[10]Lead Contact
*Correspondence: aregev@broadinstitute.org (A.R.), vkuchroo@evergrande.hms.harvard.edu (V.K.K.)
https://doi.org/10.1016/j.immuni.2019.09.005

SUMMARY

Neuroimmune interactions have emerged as critical modulators of allergic inflammation, and type 2 innate lymphoid cells (ILC2s) are an important cell type for mediating these interactions. Here, we show that ILC2s expressed both the neuropeptide calcitonin gene-related peptide (CGRP) and its receptor. CGRP potently inhibited alarmin-driven type 2 cytokine production and proliferation by lung ILC2s both *in vitro* and *in vivo*. CGRP induced marked changes in ILC2 expression programs *in vivo* and *in vitro*, attenuating alarmin-driven proliferative and effector responses. A distinct subset of ILCs scored highly for a CGRP-specific gene signature after *in vivo* alarmin stimulation, suggesting CGRP regulated this response. Finally, we observed increased ILC2 proliferation and type 2 cytokine production as well as exaggerated responses to alarmins in mice lacking the CGRP receptor. Together, these data indicate that endogenous CGRP is a critical negative regulator of ILC2 responses *in vivo*.

INTRODUCTION

Allergic asthma is characterized by chronic inflammation leading to airway hyperreactivity and remodeling after repeated allergen exposure (Lambrecht and Hammad, 2015). Type 2 T helper cells (Th2 cells) drive allergic inflammation by producing large amounts of interleukin-4 (IL-4), IL-5, and IL-13, which are important for class switching to immunoglobulin E (IgE), recruitment of eosinophils, and goblet cell hyperplasia, respectively (Lambrecht and Hammad, 2015; Yu et al., 2014). However, recent studies have highlighted the role of type 2 innate lymphoid cells (ILC2s) in the development of allergic diseases. Similar to Th2 cells, ILC2s express the transcription factor Gata3 and the type 2 cytokines IL-5 and IL-13. In contrast to Th2 cells, ILC2s are primarily found at mucosal surfaces and do not express antigen-specific receptors, and thus they cannot respond directly to pathogens or allergens. Instead, they respond to signals from the tissue microenvironment (i.e., alarmins IL-25, IL-33, or TSLP), which are released by epithelial cells upon stress or damage (Liew et al., 2016; Wallrapp et al., 2018).

The role of ILC2s in initiating and amplifying type 2 inflammation is tightly regulated to prevent exaggerated mucosal immune responses. Besides alarmins, an increasing array of factors have been shown to either positively or negatively regulate ILC2 function, including cytokines (Duerr et al., 2016; Molofsky et al., 2015; Moro et al., 2016; Motomura et al., 2014; Roediger et al., 2015), cell surface receptors (Oliphant et al., 2014; Taylor et al., 2017), and lipid mediators (Barnig et al., 2013; Krishnamoorthy et al., 2015; von Moltke et al., 2017). In particular, neuroimmune interactions are critical for regulating ILC2 function in mucosal tissues. Neurons recognize and respond to immunologically relevant molecules, including bacterial- and helminth-derived products and cytokines (Cardoso et al., 2017; Chiu et al., 2013; Talbot et al., 2015). Both peptidergic and non-peptidergic neurotransmitters regulate the function of adaptive and innate immune cells, including ILCs. The neuropeptides neuromedin U (NMU) and vasoactive intestinal peptide (VIP) both promote ILC2 effector function, whereas β_2-adrenergic receptor ligands (e.g., epinephrine) inhibit ILC2 proliferation and cytokine production, indicating that neurotransmitters can both stimulate and inhibit ILC2-driven responses (Cardoso et al., 2017; Klose et al., 2017; Moriyama et al., 2018; Nussbaum et al., 2013; Talbot et al., 2015; Wallrapp et al., 2017).

Here, we identified an additional neuroimmune pathway that modulates ILC2 responses by analyzing expression of both neuropeptides and their receptors. ILC2s expressed both the neuropeptide calcitonin gene-related peptide (CGRP) and the genes encoding its receptor chains, Ramp1 and Calcrl. We demonstrate that CGRP limited type 2 cytokine production and ILC2 proliferation and induced a regulatory gene expression profile in ILCs. In an *in vivo* model, treatment with CGRP restrained ILC2-dependent airway inflammation, while deletion of *Ramp1* promoted type 2 immune responses, indicating that CGRP is a central negative regulator of ILC2-mediated allergic inflammation.

RESULTS

ILC2s Express the CGRP Receptor Subunits *Ramp1* and *Calcrl*

To identify putative neuroimmune interactions that may modify ILC2-mediated responses, we analyzed the expression of a set of neuropeptide and neurotrophic factor receptors (Hoyer and Bartfai, 2012) (Table S1) in our previously reported single-cell RNA-sequencing (scRNA-seq) atlas of lung ILCs (Wallrapp et al., 2017). As previously shown (Cardoso et al., 2017; Klose et al., 2017; Nussbaum et al., 2013; Wallrapp et al., 2017), ILC2s expressed *Vipr2* and *Nmur1* (the receptors for VIP and NMU, respectively; Figure S1A). While most other neuropeptide and neurotrophic factor receptors were either undetectable or minimally expressed (e.g., *Ntrk1*, *Ntrk3*, and *Mc1r*; Figure S1A), *Ramp1*, *Ramp3*, and *Calcrl* were expressed in a substantial proportion of cells (Figure S1A). Calcrl and Ramp1 form the receptor for CGRP, while Ramp3 and Calcrl form the receptor for adrenomedullin (ADM) (Figure S1B) and can act as a low affinity receptor for CGRP (Russell et al., 2014).

We examined which subsets of ILCs expressed *Ramp1*, *Ramp3*, and *Calcrl* at either steady state or following treatment with IL-33 or IL-25 (Figures S1C and S1D; Wallrapp et al., 2017). All three genes were expressed by lung-resident ILCs from all conditions with broad expression of *Ramp1* (Figure S1E). In addition, *Ramp3* was highly expressed in a subset (cluster 9) of alarmin-induced ILC2s as well as in a minor subset of ILC3s (Figure S1E).

We validated these results with quantitative real-time PCR (real-time qPCR) of *Ramp1*, *Ramp3*, and *Calcrl* on lung-resident cell types. All three genes were highly expressed in naive ILC2s, consistent with our scRNA-seq data (Figure S1F). Though other immune cell populations and CD45$^-$ stromal cells also expressed *Ramp1*, *Ramp3*, and *Calcrl*, expression of *Ramp1* and *Calcrl* was highest in ILC2s compared with the other immune cell types (Figure S1F).

Lung ILC2s Express the Neuropeptide CGRP

We next investigated whether there are other cellular sources of CGRP in the lung besides neurons and neuroendocrine cells (Branchfield et al., 2016; Chiu et al., 2013; Sui et al., 2018). To test if CGRP is expressed in lung-resident immune cell populations, we used mice that express GFP under the control of the promoter of the gene encoding CGRP (*Calca*) (McCoy et al., 2012). Rare GFP$^+$ cells (<1%) were seen from most lung-resident immune cell types, while ~17% of ST2$^+$ ILC2s were GFP$^+$ at steady state (Figure S1G). IL-33 challenge did not increase the frequency of GFP$^+$ ILC2s, but their frequency increased in response to the combination of IL-33 and CGRP (Figure S1G). *Calca* was largely co-expressed in one (cluster 9) of the two subsets (clusters 2 and 9) of lung ILCs that also highly expressed *Ramp3* in scRNA-seq data (Figures S1E and S1H). ILCs also expressed several other genes encoding neurotransmitters, including *Ubl5* and neuromedin B (*Nmb*), both of which have been implicated in regulating organismal metabolism (Figure S1I; Table S1; Collier et al., 2000; Majumdar and Weber, 2011). However, *Calca* was the only one where ILCs also expressed the receptor (Figure S1A). Taken together, our data show that ILCs uniquely express both chains of the CGRP receptor and CGRP itself, indicating that this pathway may play a key role in regulating ILC responses, potentially in an autocrine or paracrine manner.

CGRP Negatively Regulates ILC2 Responses Driven by IL-33 and IL-25+NMU *In Vitro*

To investigate how CGRP affects ILC2 function, we examined its effects on ILC2s *in vitro*, either alone or with IL-33 (Figure 1A). A recent report demonstrates that CGRP enhances IL-5 production by ILC2s (Sui et al., 2018), inferring that it promotes ILC2 activation. Indeed, after 6 h, ILC2s cultured with CGRP had upregulated expression of *Il5* compared with ILC2s cultured with IL-7 alone (Figure 1B, bottom) and showed a trend toward increased expression of amphiregulin (*Areg*) (Figure S2A). In contrast, CGRP downregulated expression of *Il13*, indicating that CGRP may have a more nuanced role in regulating ILC2 responses (Figure 1B, top). Together with IL-33, CGRP led to significantly decreased *Il13* expression and significantly increased *Il5* and *Areg* expression when compared with IL-33 alone (Figures 1C and 1D). Similarly, short-term treatment with CGRP+IL-33 increased the frequency of IL-5$^+$ ILCs compared with IL-33 alone (Figure S2B), whereas the frequency of IL-13$^+$ ILC2s was significantly reduced (Figure S2C). Thus, CGRP treatment rapidly alters expression of three key effector cytokines produced by ILC2s, inducing both IL-5 and *Areg* and inhibiting IL-13.

The impact of CGRP on IL-33-induced changes in cytokine expression varied over time. After 3 days, CGRP treatment continued to promote *Areg* (Figure 1E) and repress IL-13 mRNA and protein expression (Figures 1F and 1G, top), decreasing both the frequency of IL-13$^+$ ILCs and intensity of IL-13 expression (Figure 1H, left). However, in contrast to short-term CGRP treatment, IL-5 mRNA and protein were both reduced after 3 days (Figures 1F and 1G, bottom) with significant decreases in both the frequency of IL-5-producing ILCs and the intensity of IL-5 expression (Figure 1H, right). CGRP similarly inhibited ILC2 responses to IL-25 and NMU (Figures 1I and 1J), which synergize to promote type 2 cytokine production in lung ILC2s (Wallrapp et al., 2017). Thus, over time CGRP inhibits IL-33-induced production of both IL-5 and IL-13 *in vitro* and can inhibit ILC responses to two distinct stimuli.

CGRP Inhibits IL-33-Induced ILC2 Proliferation *In Vitro*

CGRP also suppressed ILC2 proliferation. We cultured lung ILCs labeled with CellTrace Violet for 3 days with IL-7, IL-33, or IL-33+CGRP. ILC2s proliferated in response to IL-33 (Figure 1K),

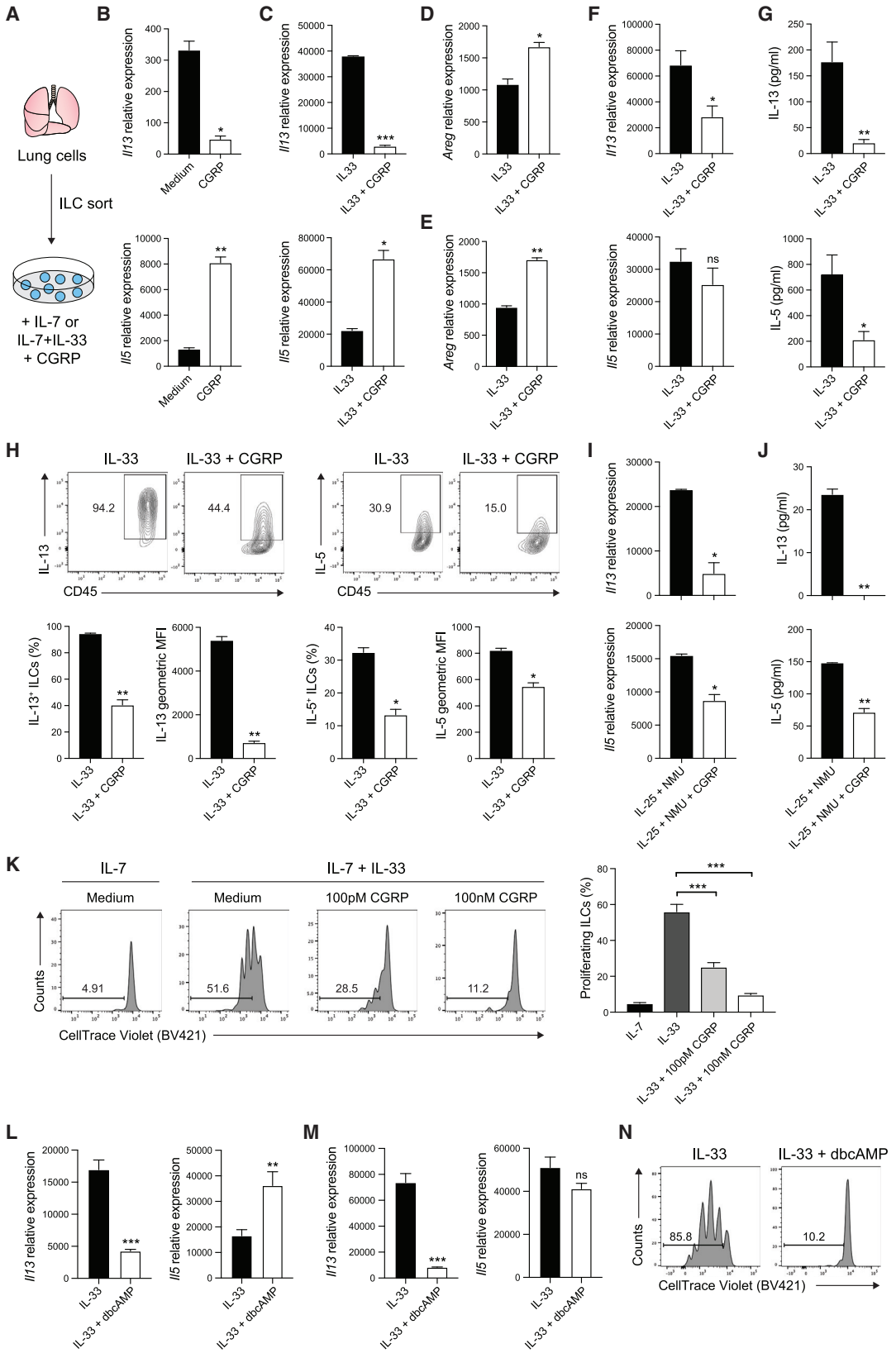

(legend on next page)

while addition of CGRP strongly inhibited IL-33-induced ILC2 proliferation in a dose-dependent manner (Figure 1K). Though ~55% of IL-33-activated ILCs divided at least once, less than 10% of ILCs proliferated in the presence of 100nM CGRP. Thus, CGRP negatively regulates IL-33-driven ILC2 proliferation and type 2 cytokine production, while promoting expression of *Areg*.

Upon binding to its receptor, CGRP induces generation of cyclic AMP (cAMP; a key second messenger) (Russell et al., 2014). To investigate whether CGRP regulates ILC2 proliferation and type 2 cytokine expression via cAMP, we cultured lung ILCs with IL-33 and cell-permeable dibutyryl-cAMP (dbcAMP). Similar to CGRP, dbcAMP increased *Areg* expression and reduced *Il13* expression, while *Il5* expression was induced at 6 h and inhibited at 3 days (Figures 1L,1M, S2D, and S2E). IL-33-induced ILC2 proliferation was also inhibited by dbcAMP (Figure 1N), indicating CGRP activation of cAMP-signaling pathways can modulate ILC2 responses.

CGRP Does Not Inhibit Inflammatory ILC2s *In Vitro*

Recent work has highlighted a distinct population of IL-25-induced inflammatory ILC2s (iILC2s) in both the lung and intestine that play an important role in host defense (Huang et al., 2018). We previously identified a distinct population (Figure S1D, cluster 8) with an iILC2-like gene expression profile—i.e., relatively high *Klrg1, Il6,* and *Il17a* expression and relatively low expression of *Il1rl1*, which encodes the IL-33 receptor ST2 (Figure 2A) (Huang et al., 2015; Huang et al., 2018; Wallrapp et al., 2017). Cluster 8 cells also had significantly lower *Ramp1* expression than other ILC2s ($p < 4.3x10^{-45}$, logistic regression, Wald test) and minimal *Ramp3* expression (Figure 2B). We confirmed reduced *Ramp1* expression in iILC2s by isolating lung-resident natural $ST2^+$ nILC2s and $KLRG1^{hi}$ $ST2^-$ iILC2s from IL-25-treated mice (Figures 2C and S3). *Ramp1* and *Calcrl* expression were extremely low in iILC2s compared with nILC2s by qPCR (Figure 2D), suggesting that iILC2s may not be inhibited by CGRP as they lack receptor expression.

We confirmed that iILC2s are less CGRP-responsive by culturing iILC2s with either IL-33 or IL-25 with or without CGRP (Figure 2E). CGRP did not inhibit IL-25- or IL-33-induced *Il5* or *Il13* expression in iILC2s (Figures 2F and 2G). Thus, while CGRP inhibits type 2 cytokine production by $ST2^+$ nILC2s, iILC2s do not express the CGRP receptor and are not inhibited by CGRP *in vitro*.

CGRP Induces Transcriptional Changes and a Revised Chromatin Landscape

We profiled how CGRP altered expression and chromatin accessibility in IL-33-activated ILC2s. By 6 h, CGRP markedly altered the chromatin landscape of ILC2s. Of the 92,814 accessible regions detected in ILC2s activated with or without CGRP, 9,760 were significantly modified by CGRP ($p < 0.05$, Wald test) (Figure 3A; Table S3). CGRP also altered the transcriptional response of ILC2s to IL-33 (Figure 3B; Table S2A) (>2,691 differentially expressed genes; FDR-adjusted $p < 0.05$, Wald test; fold change >1.5; STAR Methods), actively inducing a distinct transcriptional state: half of the differentially expressed genes were upregulated by IL-33+CGRP when compared with IL-33 alone.

Many of the transcriptionally regulated genes (e.g., *Ramp3*, *Calca*, *Il5*, and *Il13*) also had significant, consistent changes in chromatin accessibility (596 of 1,911 genes with increased expression were near regions of increased chromatin accessibility; 894 of 1,685 genes with decreased expression were near regions of decreased chromatin accessibility; $p < 1.96x10^{-194}$, hypergeometric test) (Figures 3B, 3C, and S4A). Genes with increased expression and accessibility included *Crem* (which is downstream of cAMP signaling [Foulkes et al., 1996]), *Il1rl1*, and genes associated with metabolism (e.g., *Odc1*) or hypoxia (e.g., *Hif1a*) (Figure 3B). CGRP also enhanced chromatin accessibility and transcription of *Ramp3* and *Calca*, indicating that CGRP regulates its own expression in ILC2s (Figures 3B and

Figure 1. CGRP Inhibits Type 2 Cytokine Expression and Proliferation of ILC2s *In Vitro*

(A) Lungs ILCs were isolated from C57BL/6J mice by fluorescence activated cell sorting (FACS) and cultured with IL-7 or IL-7+IL-33 with medium or CGRP.

(B and C) *Il13* and *Il5* expression in ILC2s cultured with IL-7 (B) or IL-7+IL-33 (C) with medium or CGRP for 6 h, determined by qPCR. Data points are technical replicates (n = 2). Data are representative of two independent experiments.

(D and E) *Areg* expression in ILC2s cultured for either 6 h (D) or 3 days (E), determined by qPCR. Data points are technical replicates (n = 2). Data are representative of two (D) or three (E) independent experiments.

(F) *Il13* and *Il5* expression in ILCs cultured for 3 days, determined by qPCR. Data points are averages of technical replicates from four independent experiments.

(G) IL-13 and IL-5 concentration in 3-day ILC culture supernatants, determined by LegendPlex. Data points are averages of technical replicates from four independent experiments.

(H) Expression of IL-13 and IL-5 in ILCs cultured for 3 days, analyzed by flow cytometry. Representative flow cytometry plots, frequency, and geometric mean fluorescence intensity (MFI) of IL-5 and IL-13 are shown. Data points are technical replicates (n = 2). Data are representative of two independent experiments.

(I) *Il13* and *Il5* expression in ILCs cultured with IL-25+NMU or IL-25+NMU+CGRP for 3 days, determined by qPCR. Data points are technical replicates from one experiment. Data are representative of three independent experiments.

(J) IL-13 and IL-5 concentration in 3-day ILC culture supernatants, determined by LegendPlex. Data points are technical replicates from one experiment. Data are representative of three independent experiments.

(K) CellTrace Violet-labeled ILCs cultured for 3 days, analyzed by flow cytometry. Histograms (left) show CellTrace Violet dye dilution. Graph (right) shows the frequency of proliferating ILCs from 2-3 independent experiments.

(L) *Il13* and *Il5* expression in ILC2s cultured for 6 h, determined by qPCR. Data are pooled from three independent experiments with two technical replicates each.

(M) *Il13* and *Il5* expression in ILCs cultured for 3 days, determined by qPCR. Data are pooled from three independent experiments with two technical replicates each.

(N) Cell Trace Violet-labeled ILCs were cultured for 3 days, and proliferation was analyzed by flow cytometry. Data are representative of two independent experiments.

Data shown as the mean ± SEM *p < 0.05; **p < 0.01; ***p < 0.001; ns, not significant; by either unpaired t test (B–J, L, M) or unpaired ANOVA (K). See also Figure S2.

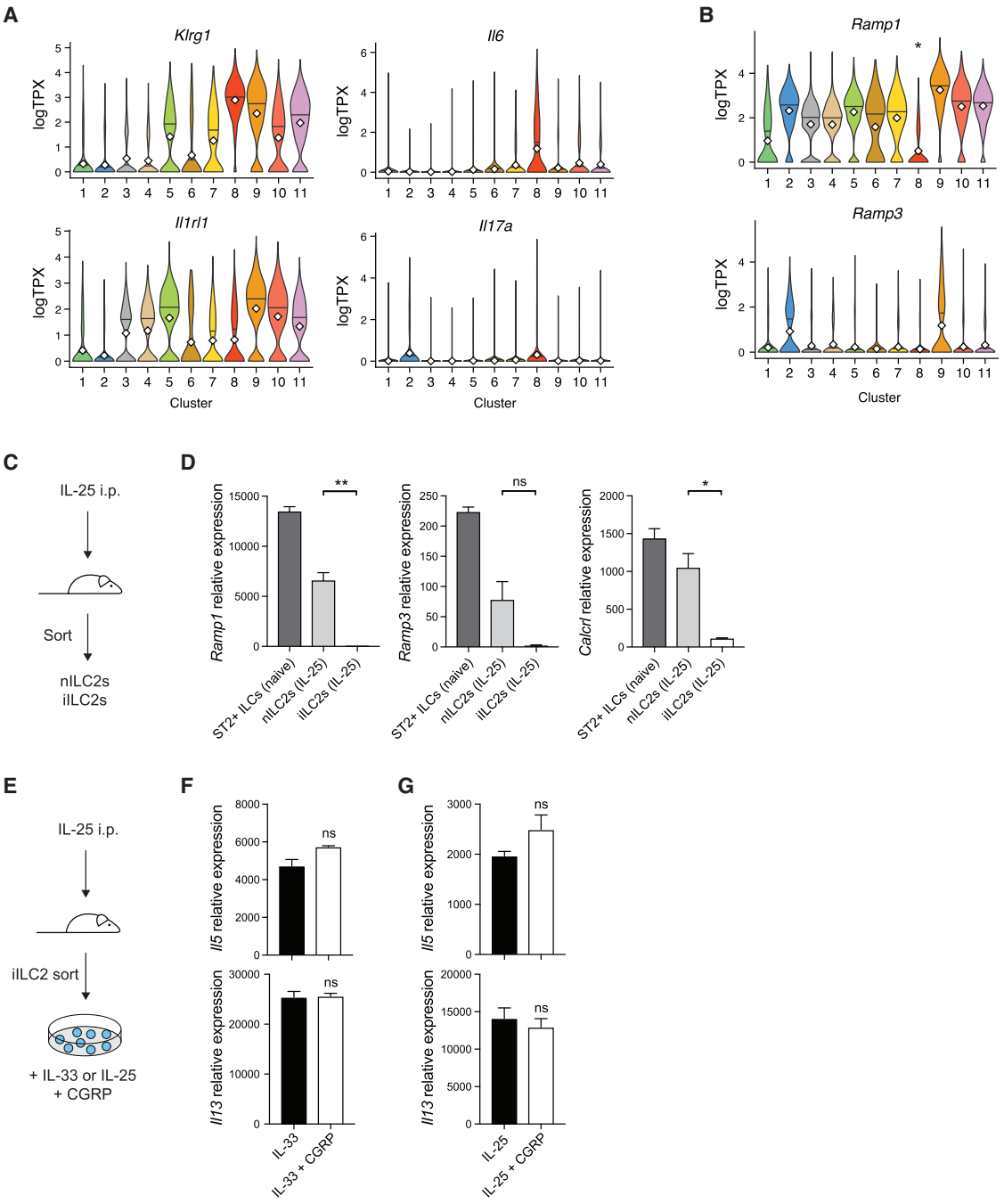

Figure 2. Inflammatory ILC2s Express Less Ramp1 and Do Not Respond to CGRP

(A and B) Expression of the indicated genes in ILCs by cluster (shown in Figure S1D) as determined by scRNA-seq. Violin plots show expression (y axis, white diamond indicates mean) of *Klrg1*, *Il6*, *Il1rl1*, and *Il17a* (A), or *Ramp1* and *Ramp3* (B) by cluster (x axis). *$p < 4.3x10^{-45}$, logistic regression, Wald test.

(C) IL-25 was given intraperitoneally for 3 consecutive days. Natural ILC2s (ST2+ KLRG1- ILCs; nILC2s) and inflammatory ILC2s (ST2- KLRG1+ ILCs; iILC2s) were then isolated.

(D) *Ramp1*, *Ramp3*, and *Calcrl* expression in different ILC subsets, determined by qPCR. Data points are technical replicates from one experiment. Data are representative of two independent experiments.

(E) iILC2s were cultured *in vitro* with IL-33, IL-33+CGRP, IL-25, or IL-25+CGRP for 6 h.

(F and G) *Il5* and *Il13* expression in iILC2s cultured with IL-33 (F) or IL-25 (G), determined by qPCR. Data points are technical replicates from one experiment. Data are representative of two independent experiments.

For (D), (F), and (G), data are shown as the mean ± SEM *$p < 0.05$; **$p < 0.01$; ns, not significant; by either unpaired ANOVA (D) or unpaired t test (F, G). See also Figure S3.

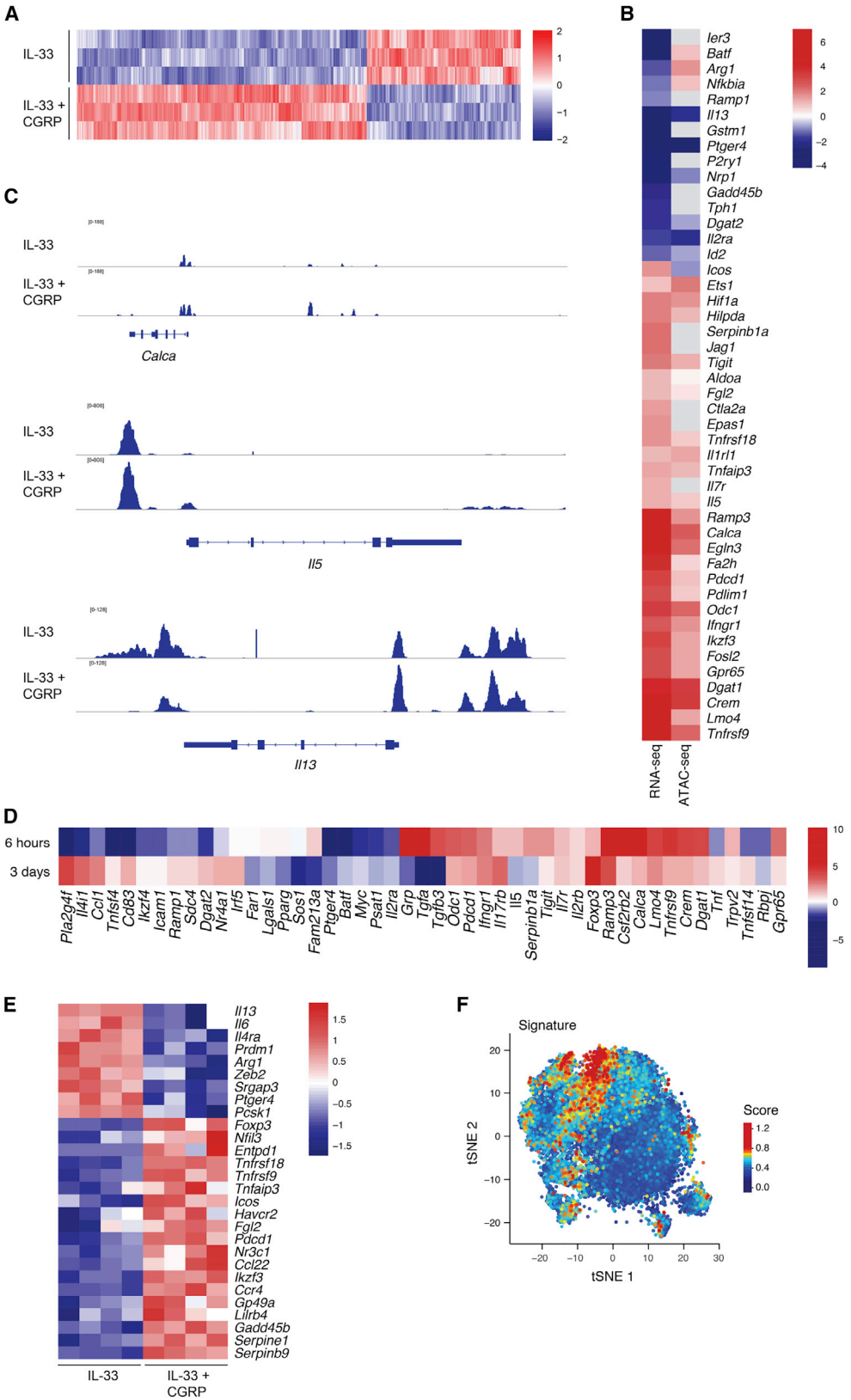

(legend on next page)

3C). Notably, CGRP enhanced chromatin accessibility of *Il5* while reducing accessibility of *Il13* (Figures 3B and 3C), mirroring the increased *Il5* expression and reduced *Il13* expression at 6 h (Figure 3B). *Ramp3*, *Calca*, *Crem*, and *Il5* were among the top 15 differentially expressed genes in ILCs treated with only CGRP for 6 h (Table S2B). Overall, the coherent CGRP-induced changes in chromatin accessibility suggest that CGRP reprograms ILC2s and leads to sustained changes in long-term gene expression.

We assessed the long-term effects of CGRP on ILC2s by analyzing gene expression profiles after 3 days of culture with CGRP and IL-33 or IL-33 alone (Figures 3D and S4B; Table S2C). A significant number of the CGRP-induced changes in expression seen at 6 h were still present with the same directionality after 3 days ($p < 2.89x10^{-150}$, hypergeometric test) (Table S2D). CGRP continued to promote a distinct transcriptional state, as 635 of 946 differentially expressed genes were upregulated by IL-33 and CGRP compared with IL-33 alone. Differentially expressed genes were enriched in gene ontology (GO) terms such as leukocyte chemotaxis (e.g., *Sell*, *S1pr1*, *Ccr7*), lipid storage (e.g., *Dgat1*, *Dgat2*, *Hilpda*), and regulation of cell activation (e.g., *Icos*, *Tnfaip3*, *Ikzf3*) (Figure S4C; Table S4; STAR Methods). However, there were exceptions where expression was induced after 6 h and reduced after 3 days (e.g., *Il5*, *Serpinb1a*, or *Tgfa*) (Figure 3D). Genes such as *Ccl1*, *Nr4a1*, or *Tnfsf4* exhibited the inverse pattern—i.e., were initially downregulated but induced later.

CGRP Induces a Regulatory Expression Program in ILC2s *In Vitro*

At both time points, CGRP-induced genes were significantly enriched in genes associated with regulatory CD4 T cells or with negative regulation of effector T cell responses, such as the cell surface molecules *Pdcd1* (PD-1), *Havcr2* (Tim-3), *Lilrb4*, *Entpd1* (CD39), and *Tnfrsf18* (GITR) ($p < 1.1x10^{-6}$, hypergeometric test) Figures 3B,3D, and 3E; Table S2; STAR Methods) (Chihara et al., 2018). Similarly, the transcription factors *Foxp3*, *Nfil3*, and *Nr3c1* and the soluble mediator *Fgl2* were upregulated (Figures 3B, 3D, and 3E). Chromatin accessibility was also increased at the loci of most of these genes (*Pdcd1*, *Tnfrsf18*, *Lilrb4*, *Entpd1*, *Nfil3*, *Nr3c1*, and *Fgl2*) (Figures 3B and S4A; Table S3). To verify that IL-33+CGRP induced Foxp3 expression at the protein level, we cultured lung ILCs from FoxP3-GFP reporter mice with IL-33+CGRP. After 3 days, a small but consistent percentage (~4%) of ILCs expressed FoxP3 versus only ~1% of ILCs cultured with IL-33 alone (Figures S5A and S5B). We also detected *Foxp3* expression in ILCs from *Rag2*$^{-/-}$ mice after culture with IL-33+CGRP (Figure S5C). Thus, CGRP may inhibit ILC2 function by inducing cell surface molecules and transcription factors associated with T cell regulation or dysfunction.

CGRP induced the regulatory program even in the absence of IL-33 (Figure S5D). Fewer differentially expressed genes were seen with CGRP alone (331 versus 946 genes), but one third of them overlapped with the CGRP+IL-33 condition (112 genes; $p < 2.0x10^{-47}$, hypergeometric test) (Table S2E), including most negatively regulatory genes (e.g., *Pdcd1*, *Lilrb4*, *Fgl2*, *Nr3c1*, and *Tnfrsf18*) (Figure S5D). GO terms associated with cell cycle progression were also enriched for downregulated, differentially expressed genes (e.g., *Mki67*, *Birc5*, *Kdm8*) (Figures S5D and S5E; Table S4), consistent with CGRP inhibiting alarmin-driven proliferation (Figure 1K). Thus, CGRP impacts ILC2 gene transcription and chromatin organization, inducing genes known to negatively regulate T cells and inhibiting genes that promote proliferation and effector function.

In Vivo Administration of CGRP Limits Alarmin-Induced Airway Inflammation

To assess whether ILC2s respond to endogenous CGRP *in vivo*, we generated a gene signature based on the transcriptional response of ILCs cultured with IL-33+CGRP *in vitro* (Table S5; STAR Methods) and used it to score cells from the previously published scRNA-seq dataset (Wallrapp et al., 2017). Cells of cluster 9, which is primarily composed of ILCs from IL-33-treated mice (1,214/1,467 cells), scored significantly higher for this signature when compared with those of the other clusters (FDR-adjusted $p < 2.2x10^{-308}$ linear regression, Wald test) (Figures 3F and S5F,; STAR Methods) and expressed more *Calca* and *Ramp3* (Figures S1E and S1H). Thus, we hypothesize that these ILCs represent a population exposed to endogenous CGRP.

To test the *in vivo* role of CGRP in ILC-driven inflammation, we treated mice with PBS, CGRP, IL-33, or IL-33+CGRP for 3 days and assessed airway inflammation (Figure 4A). While the frequency or total number of lung-resident ILCs was not altered

Figure 3. CGRP Modulates ILC Activation and Induces a Regulatory Gene Module

(A) ILC2s cultured for 6 h with IL-33 or IL-33+CGRP were profiled by assay for transposase-accessible chromatin using sequencing (ATAC-seq). Accessible regions are mapped as *Z* scores of normalized peak counts taken across columns (n = 3).

(B) ILC2s cultured for 6 h with IL-33 or IL-33+CGRP were analyzed by ATAC-seq and bulk RNA-sequencing (RNA-seq). Heatmap of significant fold changes (>1.5, color) in expression (left) of genes (rows) in ILC2s cultured with IL-33+CGRP versus IL-33 (FDR-adjusted $p < 0.05$, generalized linear regression, Wald test). Fold changes in chromatin accessibility (right) are shown for the ATAC-seq peak corresponding to the respective gene by Genomic Regions Enrichment of Annotations Tool (GREAT). When multiple peaks were assigned to a gene, the peak with the most significant change between ILC2s cultured with IL-33+CGRP versus IL-33 was shown (FDR-adjusted $p < 0.05$, Wald test).

(C) Chromatin accessibility in ILC2s treated with IL-33 (upper track of each set) or IL-33+CGRP (lower track of each set) is shown for the *Calca*, *Il5*, and *Il13* loci.

(D) ILCs cultured for 3 days with IL-33 or IL-33+CGRP were analyzed by bulk RNA-seq. Heatmap of significant fold changes (>1.5, color) in expression of genes (columns) in ILC2s cultured with IL-33+CGRP versus IL-33 for 6 h (upper row, cultured as described in B) or 3 days (lower row) (FDR-adjusted $p < 0.05$, generalized linear regression, Wald test).

(E) Heatmap of expression (color), *Z* scored by row, of selected pro-inflammatory and regulatory genes (rows) that exhibit a significant fold change (>1.5) in expression of ILCs cultured with IL-33 (left) versus IL-33+CGRP (right) for 3 days. Each column represents one replicate (FDR-adjusted $p < 0.05$, generalized linear regression, Wald test).

(F) t-distributed stochastic neighbor embedding (tSNE) plot of published single-cell RNA-seq data, as in Figures S1C and S1D, shows ILCs (dots) isolated from PBS-, IL-25-, or IL-33-treated mice, colored by score of CGRP signature.

See also Figure S4 and S5.

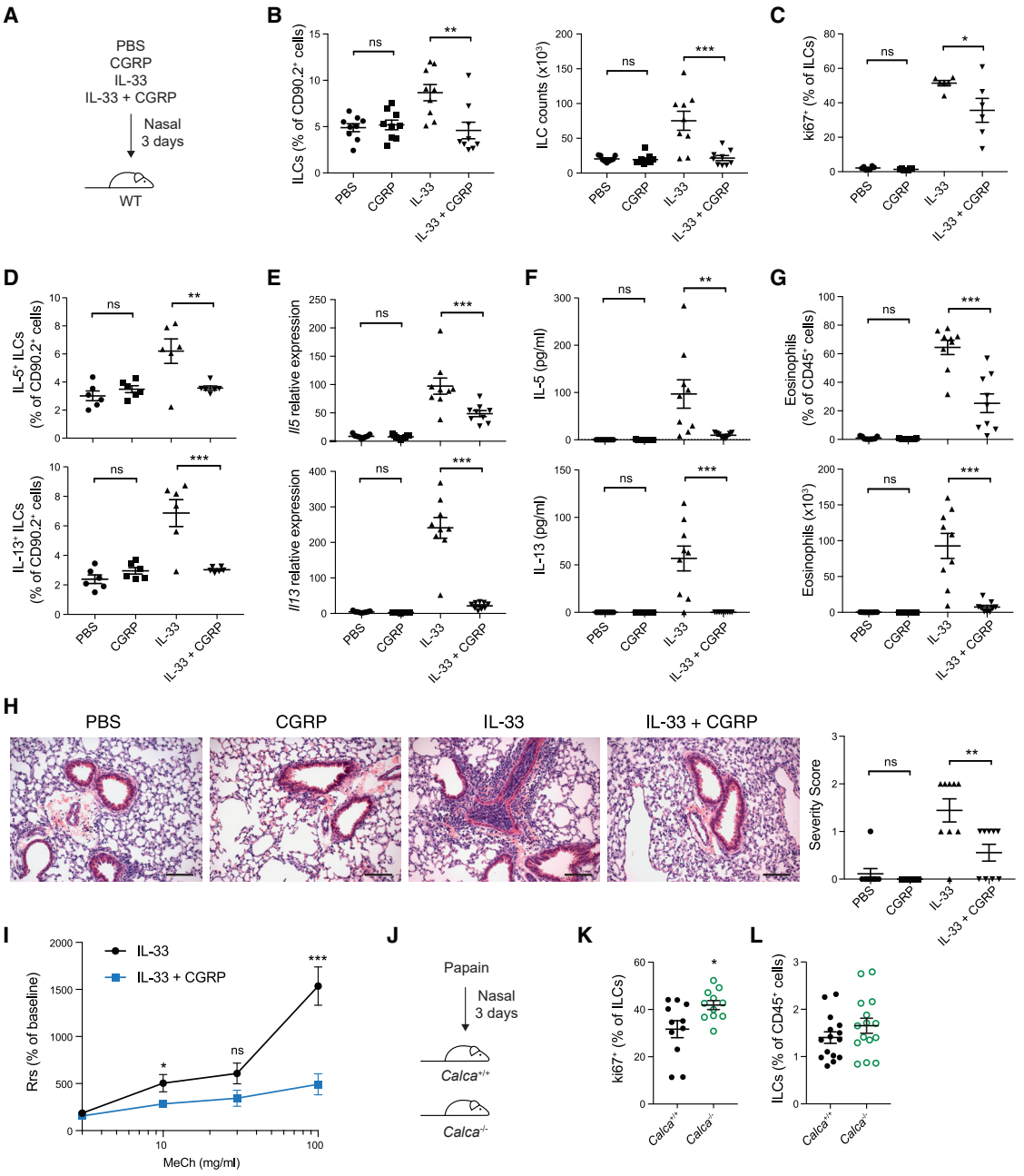

Figure 4. CGRP Dampens IL-33-Induced Airway Inflammation

(A) PBS, CGRP, IL-33, or IL-33+CGRP were administered nasally daily for 3 days.

(B) Frequency (left) and number (right) of lung ILCs, determined by flow cytometry.

(C) Frequency of Ki67$^+$ lung ILCs, determined by flow cytometry.

(D) Frequency of IL-5$^+$ and IL-13$^+$ lung ILCs, determined by flow cytometry.

(E) *Il5* and *Il13* expression in lung tissue, determined by qPCR.

(F) IL-5 and IL-13 concentration in BALF, determined by LegendPlex.

(G) Eosinophil frequency and number in BALF, determined by flow cytometry.

(H) Representative H&E stained lung sections from mice treated with PBS, CGRP, IL-33, or IL-33+CGRP (left). Graph (right) shows severity score for individual mice (n = 9) from three independent experiments. Scale bars represent 100 μm.

(I) Airway resistance was assessed in IL-33- or IL-33+CGRP-treated mice in response to methacholine challenge. Data points represent the mean of individual mice from two independent experiments (IL-33, n = 9; IL-33+CGRP, n = 9).

(J) *Calca*$^{+/+}$ and *Calca*$^{-/-}$ mice were treated nasally with papain for 3 days.

(K) Frequency of Ki67$^+$ lung ILCs, determined by flow cytometry.

(legend continued on next page)

by CGRP alone, compared with PBS, ILC frequencies and numbers were significantly reduced by IL-33+CGRP when compared with IL-33 alone, indicating that CGRP inhibits IL-33-induced ILC expansion *in vivo* (Figure 4B). The frequency of Ki67^{+} ILCs was also decreased by IL-33+CGRP compared with IL-33 alone (Figure 4C).

CGRP also inhibited production of type 2 cytokines by ILCs after IL-33 stimulation *in vivo*. Compared to IL-33 alone, CGRP and IL-33 significantly reduced the frequency of IL-5^{+} and IL-13^{+} ILCs (Figure 4D) and lung *Il5* and *Il13* transcripts (Figure 4E), while additionally IL-5 and IL-13 proteins were greatly diminished in lung homogenate and bronchoalveolar lavage fluid (BALF) (Figures 4F and S6A). The frequency and number of eosinophils in both lung tissue and BALF were also significantly decreased by CGRP (Figures 4G and S6B). Moreover, IL-33-induced perivascular and peribronchial-lymphocytic infiltrates in lung sections were reduced by CGRP (Figure 4H), and IL-33+CGRP-treated mice developed less airway hyperreactivity than mice treated only with IL-33 (Figure 4I). Thus, CGRP is a potent inhibitor of IL-33-driven inflammation *in vivo*. We also examined papain-induced ILC2 responses in *Calca*$^{+/+}$ and *Calca*$^{-/-}$ mice (Halim et al., 2012; Halim et al., 2014). Consistent with the effect of exogenous CGRP administration, there was significantly increased ILC2 proliferation and a trend toward increased ILC2 frequency in papain-treated *Calca*$^{-/-}$ mice (Figures 4J–4L).

CGRP also inhibited ILC responses induced *in vivo* by IL-25+NMU, albeit more mildly. We treated mice with IL-25, IL-25+CGRP, IL-25+NMU, or IL-25+NMU+CGRP (Figure S6C). IL-25+CGRP had no effect on ILC frequencies and numbers, but co-administration of CGRP with IL-25+NMU strongly reduced ILC frequency and number (Figure S6D). CGRP also significantly decreased IL-25+NMU-induced ILC proliferation, as assessed by Ki67 staining (Figure S6E). Compared to IL25+NMU, co-treatment with CGRP also diminished expression of type 2 cytokines at the mRNA level in the lung (Figure S6F), reduced IL-13 protein in both lung tissue and BALF, and showed trends toward reduced IL-5 protein expression (Figures S6G and S6H) and decreased BALF eosinophil frequency and number (Figure S6I). Thus, while CGRP more potently inhibits IL-33-driven ILC2 responses, it also inhibits IL-25+NMU-induced ILC activation *in vivo*.

CGRP Inhibition of ILC2s Is Independent of T Cells

To test if CGRP inhibits ILC2 activation independently of adaptive immune cells, we analyzed the effect of CGRP on IL-33-induced airway inflammation in *Rag2*$^{-/-}$ mice (Figure 5A). Total numbers of lung ILCs were significantly reduced in IL-33+CGRP-treated mice compared to IL-33 alone, and there were trends toward lower frequencies of both ILCs and Ki67^{+} ILCs (Figures 5B and 5C). Although the frequency of IL-5^{+} ILCs was not different, the frequency of IL-13^{+} ILCs was significantly lower in IL-33+CGRP-treated mice (Figure 5D). Compared with IL-33 alone, treatment with IL-33+CGRP also significantly reduced *Il5* and *Il13* transcripts in the lung (Figure 5E), IL-5 and IL-13 protein concentration in lung homogenates and BALF (Figures 5F and 5G), and eosinophil numbers in the lung and BALF (Figures 5H and 5I). Histopathological analysis also showed that IL-33+CGRP reduced lymphocytic infiltrates in lung sections of *Rag2*$^{-/-}$ mice compared with IL-33 alone (Figure 5J). Thus, CGRP negatively regulates alarmin-driven ILC2 responses independently of adaptive immunity.

CGRP Largely Reverts the IL-33-Induced Program *In Vivo*

To characterize the transcriptional response of ILC2s to CGRP at the single-cell level, we analyzed 31,053 lung ILCs from mice treated with PBS, CGRP, IL-33, or IL-33+CGRP by scRNA-seq (Figures 6A and S7A–S7D). CGRP alone had little impact on the distribution of ILCs overall (Figure 6A) and across 16 clusters (Figures 6B and 6C), while IL-33 caused a dramatic shift ($p < 5.38x10^{-132}$, Dirichlet multinomial regression, Wald test). Cells from IL-33+CGRP treated mice were largely—albeit not completely ($p < 6.38x10^{-37}$, Dirichlet multinomial regression, Wald test)—shifted back to their control distribution, including in non-ILC2 clusters (Figures 6A–6C and S7E). ILC2s from CGRP-treated mice mostly co-localized with control ILC2s, suggesting that CGRP alone minimally affected ILC2 transcriptional profiles (Figures 6A, 6C, and 6D). Three clusters (3, 4, and 9) were predominantly comprised of IL-33-treated ILC2s (84%–89%), whereas IL-33+CGRP ILC2s mostly clustered with PBS- or CGRP-treated ILC2s, indicating the extent to which CGRP inhibited ILC2 activation *in vivo* (Figures 6D and S7F).

Consistent with known effects of IL-33 relative to the PBS-dominated cluster (cluster 2), clusters 4 and 9 scored highly for a proliferative gene signature and, along with cluster 3, were more likely to express *Il13* ($p < 7.9x10^{-203}$) and *Il5* (clusters 3 and 4 only, $p < 2.1x10^{-14}$, logistic regression, Wald test) (Figures 6E, 6F, and S7G). Each of these clusters had a distinct expression profile (Figure 6G; Table S6): cluster 4 strongly upregulated genes associated with cell cycle (e.g., *Mki67*, *Cdk1*, *Birc5*), cluster 9 expressed genes associated with antigen presentation (e.g., *H2-Ab1*, *Cd74*), and cluster 3 expressed genes associated with effector ILC2s (e.g., *Arg1*, *Ly6a*, *Il5*, and *Il13*). Conversely, ILC2s from the IL-33+CGRP condition had dramatically different expression profiles from those of ILC2s from the IL-33 condition, with significantly reduced proliferative signature scores and less frequent *Il13* expression ($p < 2.2x10^{-308}$, linear and logistic regression, Wald test) (Figures 6E and 6F, Figure S7G). While IL-33+CGRP ILC2s comprised only 7%–14% of IL-33-dominated clusters, they contributed 41%–49% of cells in clusters 5, 6, and 12, which also contained PBS or CGRP ILCs (Figure S7F). Clusters 5, 6, and 12 express genes associated with tissue repair (e.g., *Areg*), cAMP signaling (e.g., *Atf3*), and several chemokines (e.g., *Cxcl1*, *Cxcl2*, *Ccl1*) (Figure 6G; Table S6).

Of note, cluster 11 highly expressed *Calca* and *Ramp3* as well as genes associated with regulatory phenotypes, consistent with our *in vitro* findings with IL-33+CGRP. These also included immune checkpoint genes (e.g., *Pdcd1*, *Tnfrsf18*,

(L) Lung ILC frequency, determined by flow cytometry.

Data points are individual mice pooled from three independent experiments (n = 9) in (B) and (E)–(G) and from two independent experiments (n = 6) in (C) and (D). Data points are individual mice pooled from three independent experiments (n = 11) in (K) and from four independent experiments (n = 15) in (L). Data are shown as the mean ± SEM *p < 0.05; **p < 0.01; ***p < 0.001; ns, not significant; by either unpaired ANOVA (B–H) or unpaired t test (I, K, L). See also Figure S6.

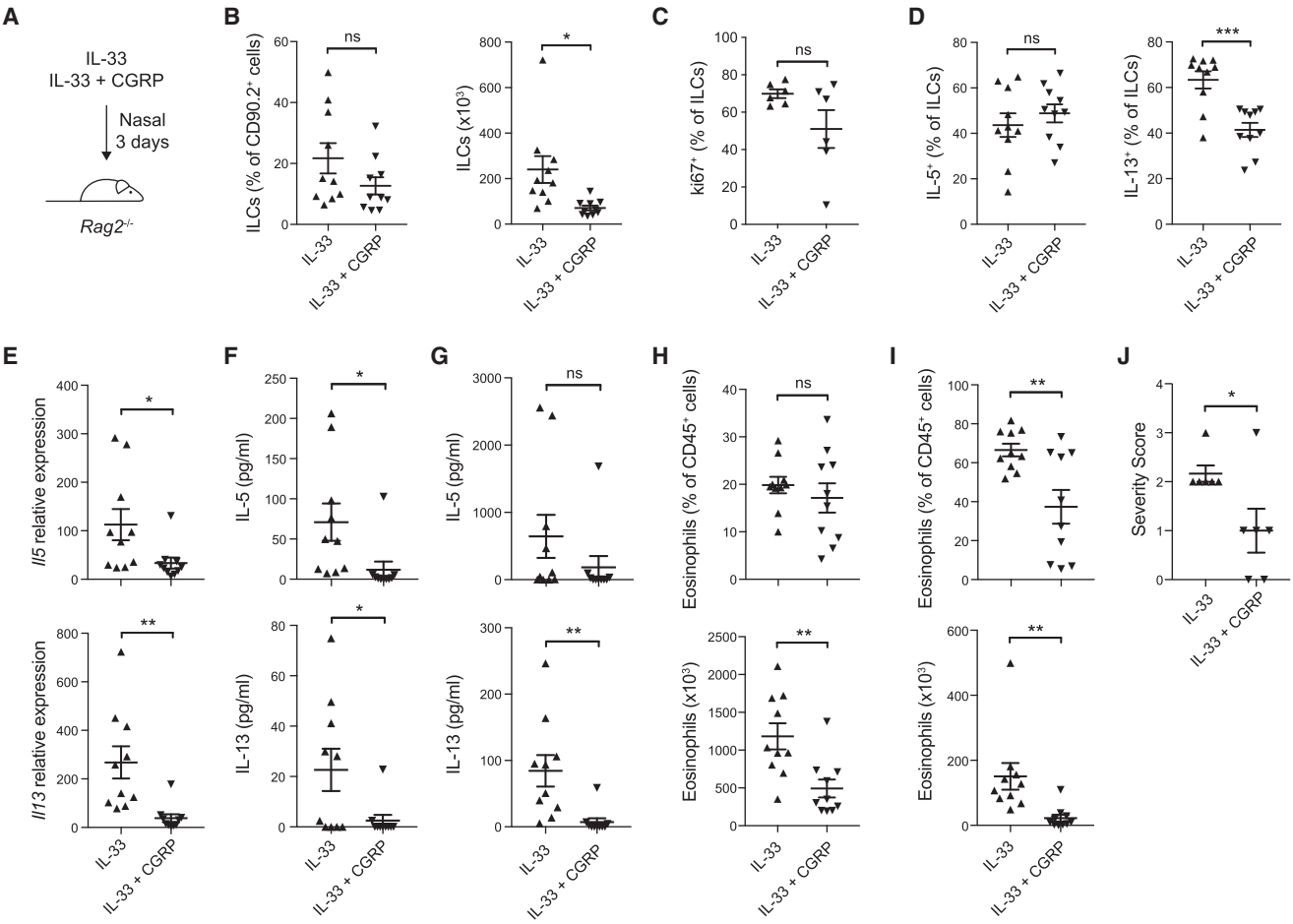

Figure 5. CGRP Negatively Regulates ILC2 Responses *In Vivo* Independent of Adaptive Immunity

(A) Nasal administration of IL-33 or IL-33+CGRP to *Rag2*$^{-/-}$ mice for 3 consecutive days.

(B) Frequency (left) and number (right) of lung ILCs, determined by flow cytometry.

(C) Frequency of Ki67^{+} ILCs, analyzed by flow cytometry.

(D) Frequency of IL-5^{+} and IL-13^{+} lung ILCs, determined by flow cytometry.

(E) *Il5* and *Il13* expression in lung tissue, determined by qPCR.

(F and G) IL-5 and IL-13 concentration in lung tissue (F) and BALF (G), determined by LegendPlex.

(H and I) Frequency and number of eosinophils in lung tissue (H) and BALF (I), determined by flow cytometry.

(J) Lung sections were scored for disease severity in a blinded manner. Graph shows severity score for individual mice (n = 6) from two independent experiments. Data points represent individual mice (n = 10) pooled from three independent experiments (B, D–I) or individual mice (n = 6) from two independent experiments (C, J). Data are shown as the mean ± SEM *p < 0.05; **p < 0.01; ***p < 0.001; ns, not significant; by unpaired t test.

Tnfrsf9, *Fgl2*, *Lilrb4a*) (Figure 6H; Table S6; Chihara et al., 2018) and cAMP signaling (*Crem*), suggesting that these ILC2s encountered CGRP *in vivo*. While ILC2s from IL-33+CGRP-treated mice are a plurality of cluster 11, ILC2s from the other conditions are also present in this cluster, suggesting that ILC2s actively respond to endogenous CGRP. We observed *Foxp3* expression in a tiny fraction of ILCs, which was significantly increased in mice treated with IL-33+CGRP compared with the other conditions ($p < 0.005$, logistic regression, LRT) (Figure S7H).

Ramp1 Is Required for Regulation of ILC2 Responses by CGRP

To investigate how endogenous CGRP regulates ILC2-mediated airway inflammation, we analyzed wild-type (WT) and *Ramp1*$^{-/-}$ mice at steady state and after IL-33 treatment. Ki67^{+} ILC frequency was significantly increased at steady state in *Ramp1*$^{-/-}$ mice compared with controls, as were the frequencies of IL-5^{+} and IL-13^{+} ILCs (Figures 7A and 7B), indicating that CGRP is an important basal regulator of ILC proliferation and cytokine production *in vivo*. The frequency and number of eosinophils were also significantly elevated in naive *Ramp1*$^{-/-}$ mice (Figure 7C). Moreover, after IL-33 challenge, *Il5* and *Il13* expression was increased in the lungs of *Ramp1*$^{-/-}$ mice as was the frequency of lung eosinophils, indicating exaggerated alarmin responses in *Ramp1*$^{-/-}$ mice (Figures 7D–7F). Finally, exogenous CGRP failed to inhibit IL-33-induced lung *Il5* and *Il13* expression, eosinophilia, and ILC2 expansion in *Ramp1*$^{-/-}$ mice, in contrast to controls (Figures 7D–7G). Thus, Ramp1 is required for CGRP to inhibit ILC2 responses *in vivo*.

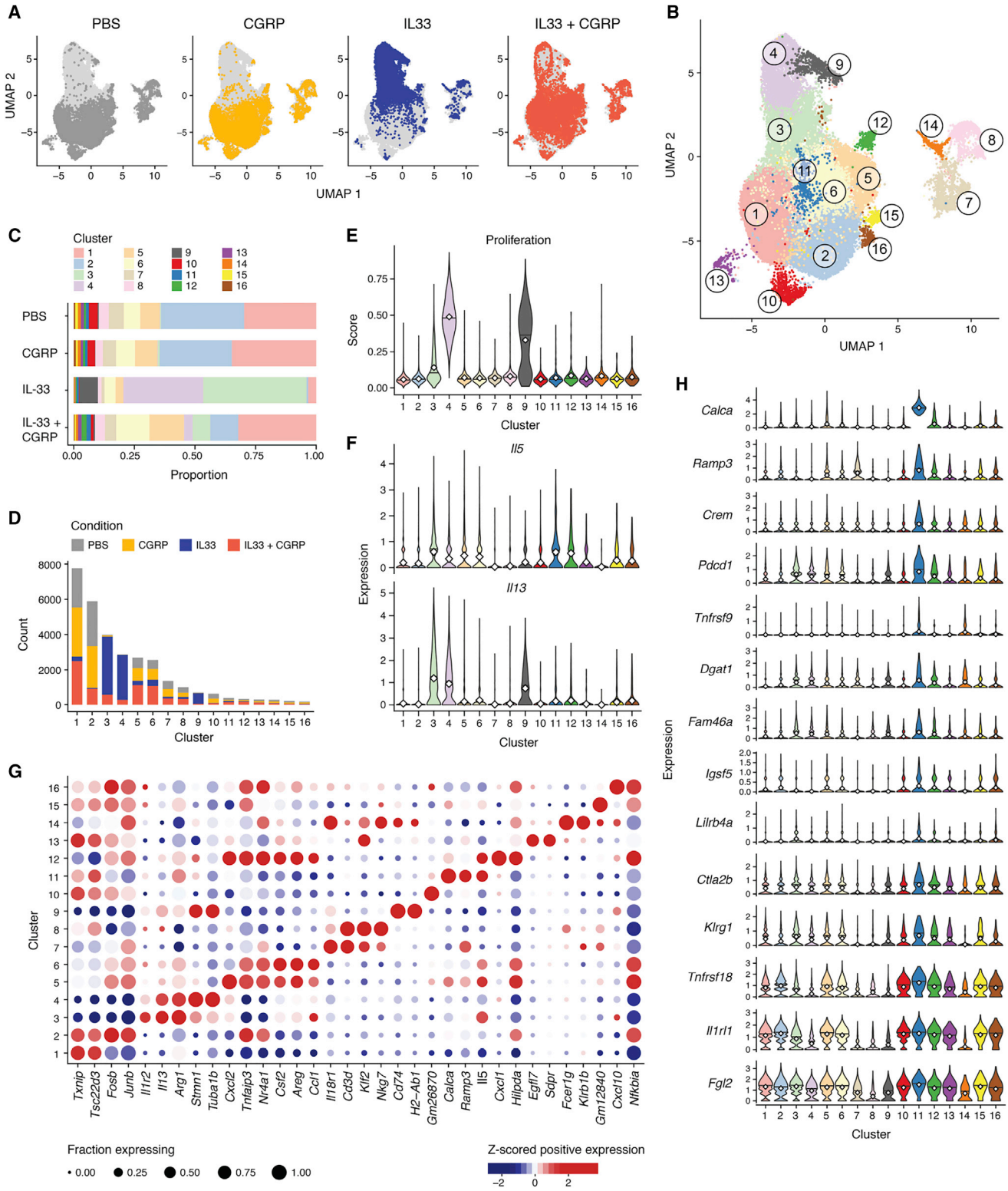

Figure 6. CGRP Inhibits Proliferative and Inflammatory Response of ILC2s to IL-33

(A–H) Uniform manifold approximation and projection (UMAP) embedding of 31,053 cells (dots) isolated from PBS-, CGRP-, IL-33-, or IL-33+CGRP-treated mice, colored by treatment condition (A) or by cluster (B). (C) Bar plot of proportions (x axis) of cells from each cluster (color) per condition (y axis). (D) Bar plot of counts (y axis) of cells from each treatment condition (color) per cluster (x axis). (E) ILC2s were scored for expression of proliferation signature genes. Violin plots show distributions of proliferation signature scores (y axis, white diamond indicates mean) for each cluster (x axis). (F) Violin plots show distributions of *Il5* and *Il13*

(legend continued on next page)

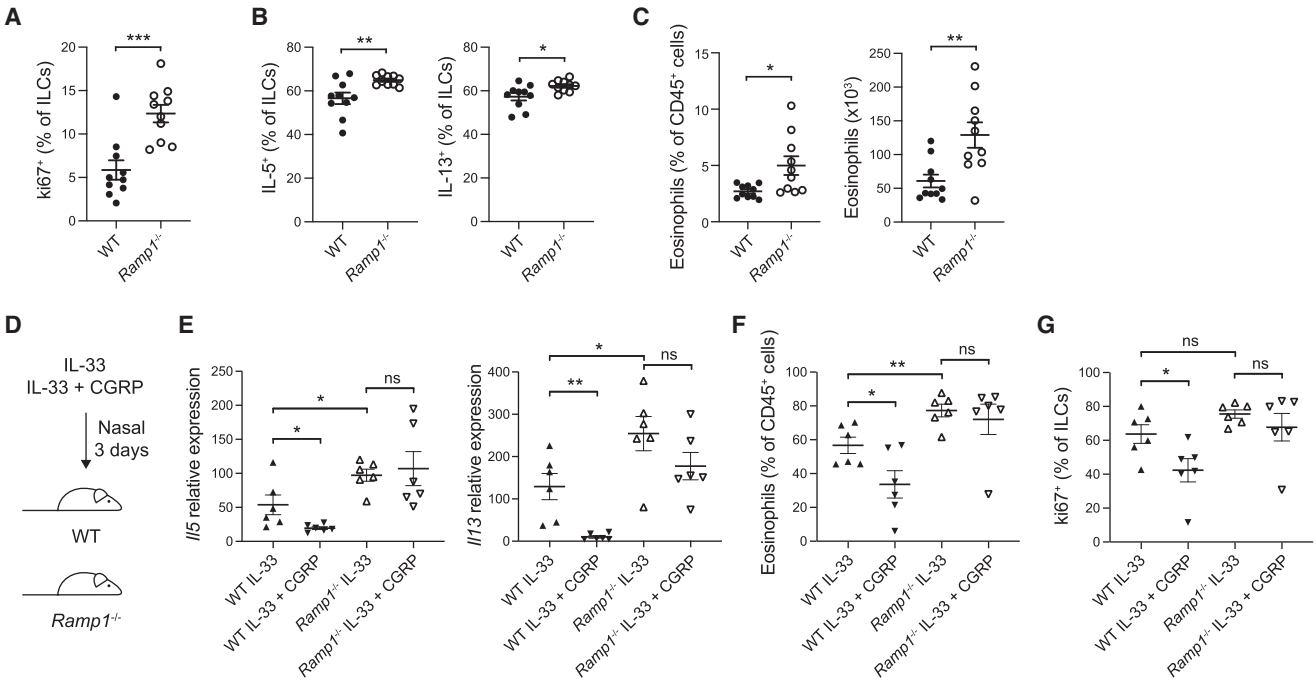

Figure 7. Increased Type 2 Immunity in *Ramp1*$^{-/-}$ Mice

(A–G) WT mice were purchased from Jackson Laboratories and co-housed with *Ramp1*$^{-/-}$ mice for at least one week. (A–C) Naive WT and *Ramp1*$^{-/-}$ mice. (A) Frequency of Ki67^{+} lung ILCs, analyzed by flow cytometry. (B) Frequency of IL-5^{+} and IL-13^{+} lung ILCs, determined by flow cytometry. (C) Lung eosinophil frequency and number, analyzed by flow cytometry. (D–G) IL-33 or IL-33+CGRP were administered nasally to WT mice or *Ramp1*$^{-/-}$ mice for 3 days. (D) Schematic illustrating experimental model. (E) *Il5* and *Il13* expression in lung tissue, determined by qPCR. (F) BALF eosinophil frequency, analyzed by flow cytometry. (G) Frequency of Ki67^{+} lung ILCs, determined by flow cytometry.

Data points are individual mice pooled from two independent experiments (n = 10, A–C or n = 6, E–G). Data are shown as the mean ± SEM *p < 0.05; **p < 0.01; ***p < 0.001; ns, not significant; by unpaired t test.

DISCUSSION

We and others recently demonstrated that neurons regulate ILC2 responses to allergens and helminths via neurotransmitters such as NMU, VIP, and epinephrine (Cardoso et al., 2017; Klose et al., 2017; Moriyama et al., 2018; Nussbaum et al., 2013; Talbot et al., 2015; Wallrapp et al., 2017). To elucidate additional neuroimmune pathways that regulate ILC2s, we analyzed neuropeptide receptor expression on ILC2s. Lung-resident ILC2s expressed both CGRP and its receptor. CGRP inhibited *in vitro* ILC2 proliferation and effector function and induced genes associated with T cell dysfunction. *In vivo*, CGRP treatment reduced acute airway inflammation by inhibiting ILC2 responses even in the absence of adaptive immune cells, indicating CGRP negatively regulates ILC2s.

Previous studies investigated the role of CGRP in regulating type 2 lung inflammation and, in contrast to our findings, reported decreased airway hyperreactivity following OVA challenge in mice lacking Ramp1 or CGRP (Aoki-Nagase et al., 2002; Li et al., 2014). Li et al. found that deleting *Calcrl* specifically in smooth muscle cells decreases airway hyperreactivity similar to observations in *Ramp1*$^{-/-}$ mice (Li et al., 2014), consistent with CGRP directly inducing human bronchial smooth muscle contraction (Springer et al., 2004). The effects of CGRP on smooth muscle therefore appear distinct from its immunomodulatory role on ILC2s. Although ILC2s highly expressed *Ramp1* at steady state and during lung inflammation, significant expression of *Ramp1* and *Calcrl* was seen in other cell types, indicating that ILCs are not the only CGRP-responsive cell type.

CGRP has pleiotropic effects on immune responses and affects both immune and non-immune cells. For instance, CGRP enhances IL-33-induced IL-5 production by ILCs in the short term, thus promoting inflammation (Sui et al., 2018). In contrast, it can also inhibit pro-inflammatory myeloid cells (Baliu-Piqué et al., 2014; Chiu et al., 2013; Harzenetter et al., 2007; Jusek et al., 2012). We have previously found that CGRP inhibits cytokine production during lung *S. aureus* infection and opsophagocytic killing of bacterial pathogens by neutrophils (Baral et al., 2018; Pinho-Ribeiro et al., 2018). While here CGRP acutely

expression (y axis, white diamond indicates mean) for each cluster (x axis). (G) Dot plot visualizes the mean expression (color), *Z* scored by column, in positively expressing cells of selected significantly differentially expressed genes (x axis, STAR Methods), per cluster (y axis). Dot size represents the proportion of cells in a cluster that express the gene. (H) Violin plots show distributions of expression (y axis, white diamond indicates mean) in each cluster (x axis, color) of selected genes (rows) that are significantly differentially expressed in Cluster 11 (blue) compared with all other cells (STAR Methods).

See also Figure S7.

enhanced ILC2 IL-5 production, it inhibited IL-13 at all time points and ILC2-mediated inflammation *in vitro* and *in vivo*.

CGRP is expressed by sensory neurons and pulmonary neuroendocrine cells (PNECs), specialized epithelial cells that sense hypoxia and produce neurotransmitters and soluble mediators (Domnik and Cutz, 2011; Linnoila, 2006). A recent study found that genetic ablation of PNECs decreases allergen-induced lung inflammation and linked this to PNEC expression of CGRP (Sui et al., 2018). However, decreased lung inflammation may be due to loss of other factors produced by PNECs. This study also reports that deletion of *Calcrl* in *Il5*-expressing cells does not alter the ILC2 frequency but does reduce the frequency of lung-infiltrating CD4+ T cells and eosinophils. Developing genetic approaches to specifically target CGRP signaling in ILC2s versus Th2 cells could provide insight into how CGRP affects these cell types.

Our finding that ILC2s express CGRP in the lung suggests that CGRP may potentially act as an autocrine or paracrine regulator or as a mechanism by which ILC2s modulate other CGRP-responsive cells. CGRP not only upregulated its own expression in ILC2s but also upregulated genes associated with inhibition of effector lymphocyte responses, including a negative regulatory gene module (*Pdcd1*, *Tnfrsf18*, *Entpd1*, *Lilbr4*, *Tnfrsf9*, and *Icos*) recently demonstrated to be induced by IL-27 in T cells (Chihara et al., 2018). The same co-inhibitory gene module, induced by different stimuli, may thus inhibit ILC2 function.

Binding of CGRP to its receptor generates cAMP (Russell et al., 2014), and chronically elevated cAMP promotes T cell anergy (Powell et al., 1999)—consistent with cell-soluble cAMP recapitulating CGRP's effects. In ILCs cultured with CGRP, we observed increased expression of genes involved in negative feedback of cAMP signaling including phosphodiesterase 4D (*Pde4d*) (which breaks down cAMP) and the transcription factor *Crem* (which can negatively regulate transcription) (Raker et al., 2016). PDE4 inhibitors have been approved for treating chronic inflammatory diseases, such as atopic dermatitis and chronic obstructive pulmonary disease, providing additional evidence that increases in intracellular cAMP inhibit inflammation (Li et al., 2018). Additionally, β_2 adrenergic receptor agonists, which also increase cAMP, have recently been shown to dampen ILC2 type 2 cytokine production and proliferation (Moriyama et al., 2018). In contrast, NMU receptor 1 (Nmur1) signals via $G_{\alpha q}$ proteins that induce calcium influx and activate phospholipase C, resulting in ILC2 stimulation (Cardoso et al., 2017; Klose et al., 2017). These data suggest that the modulation of cAMP is a critical pathway by which CGRP inhibits ILC2 activation.

Finally, our data show that by negatively regulating ILC2 responses, CGRP limits acute airway inflammation. Elucidating the role of CGRP in chronic lung inflammation will be an important area of future research, particularly in light of the recent approval of humanized monoclonal antibodies that inhibit either CGRP or the CGRP receptor (Goadsby et al., 2017; Silberstein et al., 2017). Although no asthma-related adverse events were reported in the phase 3 clinical trials of these antibodies (Goadsby et al., 2017; Silberstein et al., 2017), the possibility that these agents could enhance ILC2 responses and promote type 2 inflammation clearly warrants close monitoring as they enter widespread clinical use. Our study also highlights that activation of the CGRP receptor may represent a therapeutic strategy in allergic diseases.

STAR★METHODS

Detailed methods are provided in the online version of this paper and include the following:

- KEY RESOURCES TABLE
- LEAD CONTACT AND MATERIALS AVAILABILITY
- EXPERIMENTAL MODEL AND SUBJECT DETAILS
  - Animals
  - Primary Cell Culture
- METHOD DETAILS
  - Isolation of lung cells for fluorescence-activated cell sorting
  - Culture of innate lymphoid cells
  - Proliferation assay
  - Airway inflammation
  - RNA isolation and cDNA synthesis
  - Bead-based immunoassay
  - Methacholine assay
  - Histology
  - ATAC-seq
  - ATAC-seq data processing
  - Previously published single-cell RNA-Seq data
  - Bulk RNA-seq
  - Bulk RNA-seq data processing
  - Bulk RNA-seq analysis
  - CGRP response gene signature derivation
  - Gene signature scoring and analysis
  - New single-cell RNA-seq
- QUANTIFICATION AND STATISTICAL ANALYSIS
- DATA AND CODE AVAILABILITY

SUPPLEMENTAL INFORMATION

Supplemental Information can be found online at https://doi.org/10.1016/j.immuni.2019.09.005.

ACKNOWLEDGMENTS

We thank Junrong Xia, Guangli Zhu, Dan Dubinsky, Deneen Kozoriz, Helene Stroh, and the Dana Farber Cancer Institute Rodent Histopathology Core for technical assistance. Mark Zylka and Eric McCoy (University of North Carolina) originally generated the CGRP-GFP reporter mice. Felipe Pinho-Ribeiro bred the mice at Harvard Medical School. A.W. is a PhD student who is jointly supervised by V.K.K. and Hans-Martin Jäck (Friedrich-Alexander University of Erlangen-Nürnberg, Erlangen, Germany) and has been supported by a Boehringer Ingelheim Fonds PhD fellowship. P.R.B. (1K08AI123516), R.E.A. (1K08HL130540), P.I.T. (F32AI138458), B.D.L. (R01 HL122531), I.M.C. (R01 AI130019), and V.K.K. (R01 AI139536) are supported by the NIH. A.R. is supported by the Howard Hughes Medical Institute. We also acknowledge the support of the Food Allergy Scientific Initiative (A.R. and V.K.K.) and the Klarman Cell Observatory (A.R.) at the Broad Institute. A.R. is an HHMI investigator.

AUTHOR CONTRIBUTIONS

P.R.B. and V.K.K. conceived the study. A.W., P.R.B., S.-J.R., V.K.K., and A.R. designed the experiments and interpreted the results. A.W., P.R.B., and S.K. performed and analyzed functional biological experiments with assistance from P.K. S.J.R. designed and performed the computational analysis with

assistance from C.L. and R.H.H. E.C. performed bulk-RNA-seq. A.S. performed ATAC-seq, and P.I.T. analyzed the data. R.A.E. and B.D.L. assisted with measuring airway resistance. K.T. generated *Ramp1*$^{-/-}$ mice. R.J.X. provided scientific advice for the project. I.C. provided CGRP-GFP mice and neuro-immunology expertise. A.W., P.R.B., and S.J.R. wrote the manuscript. A.R. and V.K.K. edited the manuscript with input from all authors.

DECLARATION OF INTERESTS

A.R. is an SAB member of ThermoFisher Scientific, Neogene Therapeutics, and Syros Pharmaceuticals. A.R. and V.K.K. are cofounders of and equity holders in Celsius Therapeutics. A.W., P.R.B., S.-J.R., A.R., and V.K.K. are co-inventors on US provisional patent application no. 62/667,381, and A.R. and R.J.X. are co-inventors on US provisional patent application no. 62/818,404, which are both filed by The Broad Institute relating to CGRP signaling modulation. All other authors declare no competing interests.

Received: March 28, 2019
Revised: June 19, 2019
Accepted: September 9, 2019
Published: October 8, 2019

REFERENCES

Aoki-Nagase, T., Nagase, T., Oh-Hashi, Y., Shindo, T., Kurihara, Y., Yamaguchi, Y., Yamamoto, H., Tomita, T., Ohga, E., Nagai, R., et al. (2002). Attenuation of antigen-induced airway hyperresponsiveness in CGRP-deficient mice. Am. J. Physiol. Lung Cell. Mol. Physiol. *283*, L963–L970.

Baliu-Piqué, M., Jusek, G., and Holzmann, B. (2014). Neuroimmunological communication via CGRP promotes the development of a regulatory phenotype in TLR4-stimulated macrophages. Eur. J. Immunol. *44*, 3708–3716.

Baral, P., Umans, B.D., Li, L., Wallrapp, A., Bist, M., Kirschbaum, T., Wei, Y., Zhou, Y., Kuchroo, V.K., Burkett, P.R., et al. (2018). Nociceptor sensory neurons suppress neutrophil and γδ T cell responses in bacterial lung infections and lethal pneumonia. Nat. Med. *24*, 417–426.

Barnig, C., Cernadas, M., Dutile, S., Liu, X., Perrella, M.A., Kazani, S., Wechsler, M.E., Israel, E., and Levy, B.D. (2013). Lipoxin A4 regulates natural killer cell and type 2 innate lymphoid cell activation in asthma. Sci. Transl. Med. *5*, 174ra26.

Bettelli, E., Carrier, Y., Gao, W., Korn, T., Strom, T.B., Oukka, M., Weiner, H.L., and Kuchroo, V.K. (2006). Reciprocal developmental pathways for the generation of pathogenic effector TH17 and regulatory T cells. Nature *441*, 235–238.

Branchfield, K., Nantie, L., Verheyden, J.M., Sui, P., Wienhold, M.D., and Sun, X. (2016). Pulmonary neuroendocrine cells function as airway sensors to control lung immune response. Science *351*, 707–710.

Bray, N.L., Pimentel, H., Melsted, P., and Pachter, L. (2016). Near-optimal probabilistic RNA-seq quantification. Nat. Biotechnol. *34*, 525–527.

Butler, A., Hoffman, P., Smibert, P., Papalexi, E., and Satija, R. (2018). Integrating single-cell transcriptomic data across different conditions, technologies, and species. Nat. Biotechnol. *36*, 411–420.

Cardoso, V., Chesné, J., Ribeiro, H., García-Cassani, B., Carvalho, T., Bouchery, T., Shah, K., Barbosa-Morais, N.L., Harris, N., and Veiga-Fernandes, H. (2017). Neuronal regulation of type 2 innate lymphoid cells via neuromedin U. Nature *549*, 277–281.

Chihara, N., Madi, A., Kondo, T., Zhang, H., Acharya, N., Singer, M., Nyman, J., Marjanovic, N.D., Kowalczyk, M.S., Wang, C., et al. (2018). Induction and transcriptional regulation of the co-inhibitory gene module in T cells. Nature *558*, 454–459.

Chiu, I.M., Heesters, B.A., Ghasemlou, N., Von Hehn, C.A., Zhao, F., Tran, J., Wainger, B., Strominger, A., Muralidharan, S., Horswill, A.R., et al. (2013). Bacteria activate sensory neurons that modulate pain and inflammation. Nature *501*, 52–57.

Collier, G.R., McMillan, J.S., Windmill, K., Walder, K., Tenne-Brown, J., de Silva, A., Trevaskis, J., Jones, S., Morton, G.J., Lee, S., et al. (2000). Beacon: a novel gene involved in the regulation of energy balance. Diabetes *49*, 1766–1771.

Corces, M.R., Buenrostro, J.D., Wu, B., Greenside, P.G., Chan, S.M., Koenig, J.L., Snyder, M.P., Pritchard, J.K., Kundaje, A., Greenleaf, W.J., et al. (2016). Lineage-specific and single-cell chromatin accessibility charts human hematopoiesis and leukemia evolution. Nat. Genet. *48*, 1193–1203.

Domnik, N.J., and Cutz, E. (2011). Pulmonary neuroepithelial bodies as airway sensors: putative role in the generation of dyspnea. Curr. Opin. Pharmacol. *11*, 211–217.

Duerr, C.U., McCarthy, C.D., Mindt, B.C., Rubio, M., Meli, A.P., Pothlichet, J., Eva, M.M., Gauchat, J.F., Qureshi, S.T., Mazer, B.D., et al. (2016). Type I interferon restricts type 2 immunopathology through the regulation of group 2 innate lymphoid cells. Nat. Immunol. *17*, 65–75.

Foulkes, N.S., Borjigin, J., Snyder, S.H., and Sassone-Corsi, P. (1996). Transcriptional control of circadian hormone synthesis via the CREM feedback loop. Proc. Natl. Acad. Sci. USA *93*, 14140–14145.

Goadsby, P.J., Reuter, U., Hallström, Y., Broessner, G., Bonner, J.H., Zhang, F., Sapra, S., Picard, H., Mikol, D.D., and Lenz, R.A. (2017). A Controlled Trial of Erenumab for Episodic Migraine. N. Engl. J. Med. *377*, 2123–2132.

Hafemeister, C., and Satija, R. (2019). Normalization and variance stabilization of single-cell RNA-seq data using regularized negative binomial regression. bioRxiv. https://doi.org/10.1101/576827.

Halim, T.Y., Krauss, R.H., Sun, A.C., and Takei, F. (2012). Lung natural helper cells are a critical source of Th2 cell-type cytokines in protease allergen-induced airway inflammation. Immunity *36*, 451–463.

Halim, T.Y., Steer, C.A., Mathä, L., Gold, M.J., Martinez-Gonzalez, I., McNagny, K.M., McKenzie, A.N., and Takei, F. (2014). Group 2 innate lymphoid cells are critical for the initiation of adaptive T helper 2 cell-mediated allergic lung inflammation. Immunity *40*, 425–435.

Harzenetter, M.D., Novotny, A.R., Gais, P., Molina, C.A., Altmayr, F., and Holzmann, B. (2007). Negative regulation of TLR responses by the neuropeptide CGRP is mediated by the transcriptional repressor ICER. J. Immunol. *179*, 607–615.

Hoyer, D., and Bartfai, T. (2012). Neuropeptides and neuropeptide receptors: drug targets, and peptide and non-peptide ligands: a tribute to Prof. Dieter Seebach. Chem. Biodivers. *9*, 2367–2387.

Huang, Y., Guo, L., Qiu, J., Chen, X., Hu-Li, J., Siebenlist, U., Williamson, P.R., Urban, J.F., Jr., and Paul, W.E. (2015). IL-25-responsive, lineage-negative KLRG1(hi) cells are multipotential 'inflammatory' type 2 innate lymphoid cells. Nat. Immunol. *16*, 161–169.

Huang, Y., Mao, K., Chen, X., Sun, M.A., Kawabe, T., Li, W., Usher, N., Zhu, J., Urban, J.F., Jr., Paul, W.E., and Germain, R.N. (2018). S1P-dependent interorgan trafficking of group 2 innate lymphoid cells supports host defense. Science *359*, 114–119.

Jusek, G., Reim, D., Tsujikawa, K., and Holzmann, B. (2012). Deficiency of the CGRP receptor component RAMP1 attenuates immunosuppression during the early phase of septic peritonitis. Immunobiology *217*, 761–767.

Klose, C.S.N., Mahlakõiv, T., Moeller, J.B., Rankin, L.C., Flamar, A.L., Kabata, H., Monticelli, L.A., Moriyama, S., Putzel, G.G., Rakhilin, N., et al. (2017). The neuropeptide neuromedin U stimulates innate lymphoid cells and type 2 inflammation. Nature *549*, 282–286.

Krishnamoorthy, N., Burkett, P.R., Dalli, J., Abdulnour, R.E., Colas, R., Ramon, S., Phipps, R.P., Petasis, N.A., Kuchroo, V.K., Serhan, C.N., and Levy, B.D. (2015). Cutting edge: maresin-1 engages regulatory T cells to limit type 2 innate lymphoid cell activation and promote resolution of lung inflammation. J. Immunol. *194*, 863–867.

Lambrecht, B.N., and Hammad, H. (2015). The immunology of asthma. Nat. Immunol. *16*, 45–56.

Lee, J., Christoforo, G., Christoforo, G., Foo, C.S., Probert, C., Kundaje, A., Boley, N., kohpangwei, Dacre, M., and Kim, D. (2016). kundajelab/atac_dnase_pipelines: 0.3.3. https://doi.org/10.5281/zenodo.211733.

Li, M., Wetzel-Strong, S.E., Hua, X., Tilley, S.L., Oswald, E., Krummel, M.F., and Caron, K.M. (2014). Deficiency of RAMP1 attenuates antigen-induced airway hyperresponsiveness in mice. PLoS ONE *9*, e102356.

Li, H., Zuo, J., and Tang, W. (2018). Phosphodiesterase-4 Inhibitors for the Treatment of Inflammatory Diseases. Front. Pharmacol. *9*, 1048.

Liew, F.Y., Girard, J.P., and Turnquist, H.R. (2016). Interleukin-33 in health and disease. Nat. Rev. Immunol. *16*, 676–689.

Linnoila, R.I. (2006). Functional facets of the pulmonary neuroendocrine system. Lab. Invest. *86*, 425–444.

Love, M.I., Huber, W., and Anders, S. (2014). Moderated estimation of fold change and dispersion for RNA-seq data with DESeq2. Genome Biol. *15*, 550.

Majumdar, I.D., and Weber, H.C. (2011). Biology of mammalian bombesin-like peptides and their receptors. Curr. Opin. Endocrinol. Diabetes Obes. *18*, 68–74.

McCoy, E.S., Taylor-Blake, B., and Zylka, M.J. (2012). CGRPα-expressing sensory neurons respond to stimuli that evoke sensations of pain and itch. PLoS ONE *7*, e36355.

McLean, C.Y., Bristor, D., Hiller, M., Clarke, S.L., Schaar, B.T., Lowe, C.B., Wenger, A.M., and Bejerano, G. (2010). GREAT improves functional interpretation of cis-regulatory regions. Nat. Biotechnol. *28*, 495–501.

Molofsky, A.B., Van Gool, F., Liang, H.E., Van Dyken, S.J., Nussbaum, J.C., Lee, J., Bluestone, J.A., and Locksley, R.M. (2015). Interleukin-33 and Interferon-γ Counter-Regulate Group 2 Innate Lymphoid Cell Activation during Immune Perturbation. Immunity *43*, 161–174.

Moriyama, S., Brestoff, J.R., Flamar, A.L., Moeller, J.B., Klose, C.S.N., Rankin, L.C., Yudanin, N.A., Monticelli, L.A., Putzel, G.G., Rodewald, H.R., and Artis, D. (2018). β_2-adrenergic receptor-mediated negative regulation of group 2 innate lymphoid cell responses. Science *359*, 1056–1061.

Moro, K., Kabata, H., Tanabe, M., Koga, S., Takeno, N., Mochizuki, M., Fukunaga, K., Asano, K., Betsuyaku, T., and Koyasu, S. (2016). Interferon and IL-27 antagonize the function of group 2 innate lymphoid cells and type 2 innate immune responses. Nat. Immunol. *17*, 76–86.

Motomura, Y., Morita, H., Moro, K., Nakae, S., Artis, D., Endo, T.A., Kuroki, Y., Ohara, O., Koyasu, S., and Kubo, M. (2014). Basophil-derived interleukin-4 controls the function of natural helper cells, a member of ILC2s, in lung inflammation. Immunity *40*, 758–771.

Nussbaum, J.C., Van Dyken, S.J., von Moltke, J., Cheng, L.E., Mohapatra, A., Molofsky, A.B., Thornton, E.E., Krummel, M.F., Chawla, A., Liang, H.E., and Locksley, R.M. (2013). Type 2 innate lymphoid cells control eosinophil homeostasis. Nature *502*, 245–248.

Oh-hashi, Y., Shindo, T., Kurihara, Y., Imai, T., Wang, Y., Morita, H., Imai, Y., Kayaba, Y., Nishimatsu, H., Suematsu, Y., et al. (2001). Elevated sympathetic nervous activity in mice deficient in alphaCGRP. Circ. Res. *89*, 983–990.

Oliphant, C.J., Hwang, Y.Y., Walker, J.A., Salimi, M., Wong, S.H., Brewer, J.M., Englezakis, A., Barlow, J.L., Hams, E., Scanlon, S.T., et al. (2014). MHCII-mediated dialog between group 2 innate lymphoid cells and CD4(+) T cells potentiates type 2 immunity and promotes parasitic helminth expulsion. Immunity *41*, 283–295.

Picelli, S., Faridani, O.R., Björklund, A.K., Winberg, G., Sagasser, S., and Sandberg, R. (2014). Full-length RNA-seq from single cells using Smart-seq2. Nat. Protoc. *9*, 171–181.

Pinho-Ribeiro, F.A., Baddal, B., Haarsma, R., O'Seaghdha, M., Yang, N.J., Blake, K.J., Portley, M., Verri, W.A., Dale, J.B., Wessels, M.R., and Chiu, I.M. (2018). Blocking Neuronal Signaling to Immune Cells Treats Streptococcal Invasive Infection. Cell *173*, 1083–1097.e22.

Powell, J.D., Lerner, C.G., and Schwartz, R.H. (1999). Inhibition of cell cycle progression by rapamycin induces T cell clonal anergy even in the presence of costimulation. J. Immunol. *162*, 2775–2784.

Quinlan, A.R., and Hall, I.M. (2010). BEDTools: a flexible suite of utilities for comparing genomic features. Bioinformatics *26*, 841–842.

Raker, V.K., Becker, C., and Steinbrink, K. (2016). The cAMP Pathway as Therapeutic Target in Autoimmune and Inflammatory Diseases. Front. Immunol. *7*, 123.

Robinson, J.T., Thorvaldsdóttir, H., Wenger, A.M., Zehir, A., and Mesirov, J.P. (2017). Variant Review with the Integrative Genomics Viewer. Cancer Res. *77*, e31–e34.

Roediger, B., Kyle, R., Tay, S.S., Mitchell, A.J., Bolton, H.A., Guy, T.V., Tan, S.Y., Forbes-Blom, E., Tong, P.L., Koller, Y., et al. (2015). IL-2 is a critical regulator of group 2 innate lymphoid cell function during pulmonary inflammation. The Journal of allergy and clinical immunology *136*, 1653–1663 e1657.

Russell, F.A., King, R., Smillie, S.J., Kodji, X., and Brain, S.D. (2014). Calcitonin gene-related peptide: physiology and pathophysiology. Physiol. Rev. *94*, 1099–1142.

Silberstein, S.D., Dodick, D.W., Bigal, M.E., Yeung, P.P., Goadsby, P.J., Blankenbiller, T., Grozinski-Wolff, M., Yang, R., Ma, Y., and Aycardi, E. (2017). Fremanezumab for the Preventive Treatment of Chronic Migraine. N. Engl. J. Med. *377*, 2113–2122.

Soneson, C., Love, M.I., and Robinson, M.D. (2015). Differential analyses for RNA-seq: transcript-level estimates improve gene-level inferences. F1000Res. *4*, 1521.

Springer, J., Amadesi, S., Trevisani, M., Harrison, S., Dinh, Q.T., McGregor, G.P., Fischer, A., Geppetti, P., and Groneberg, D.A. (2004). Effects of alpha calcitonin gene-related peptide in human bronchial smooth muscle and pulmonary artery. Regul. Pept. *118*, 127–134.

Sui, P., Wiesner, D.L., Xu, J., Zhang, Y., Lee, J., Van Dyken, S., Lashua, A., Yu, C., Klein, B.S., Locksley, R.M., et al. (2018). Pulmonary neuroendocrine cells amplify allergic asthma responses. Science *360*, eaan8546.

Talbot, S., Abdulnour, R.E., Burkett, P.R., Lee, S., Cronin, S.J., Pascal, M.A., Laedermann, C., Foster, S.L., Tran, J.V., Lai, N., et al. (2015). Silencing Nociceptor Neurons Reduces Allergic Airway Inflammation. Neuron *87*, 341–354.

Taylor, S., Huang, Y., Mallett, G., Stathopoulou, C., Felizardo, T.C., Sun, M.A., Martin, E.L., Zhu, N., Woodward, E.L., Elias, M.S., et al. (2017). PD-1 regulates KLRG1$^+$ group 2 innate lymphoid cells. J. Exp. Med. *214*, 1663–1678.

Tsujikawa, K., Yayama, K., Hayashi, T., Matsushita, H., Yamaguchi, T., Shigeno, T., Ogitani, Y., Hirayama, M., Kato, T., Fukada, S., et al. (2007). Hypertension and dysregulated proinflammatory cytokine production in receptor activity-modifying protein 1-deficient mice. Proc. Natl. Acad. Sci. USA *104*, 16702–16707.

von Moltke, J., O'Leary, C.E., Barrett, N.A., Kanaoka, Y., Austen, K.F., and Locksley, R.M. (2017). Leukotrienes provide an NFAT-dependent signal that synergizes with IL-33 to activate ILC2s. J. Exp. Med. *214*, 27–37.

Wallrapp, A., Riesenfeld, S.J., Burkett, P.R., Abdulnour, R.E., Nyman, J., Dionne, D., Hofree, M., Cuoco, M.S., Rodman, C., Farouq, D., et al. (2017). The neuropeptide NMU amplifies ILC2-driven allergic lung inflammation. Nature *549*, 351–356.

Wallrapp, A., Riesenfeld, S.J., Burkett, P.R., and Kuchroo, V.K. (2018). Type 2 innate lymphoid cells in the induction and resolution of tissue inflammation. Immunol. Rev. *286*, 53–73.

Wolf, F.A., Angerer, P., and Theis, F.J. (2018). SCANPY: large-scale single-cell gene expression data analysis. Genome Biol. *19*, 15.

Yu, G., Wang, L.G., Han, Y., and He, Q.Y. (2012). clusterProfiler: an R package for comparing biological themes among gene clusters. OMICS *16*, 284–287.

Yu, S., Kim, H.Y., Chang, Y.J., DeKruyff, R.H., and Umetsu, D.T. (2014). Innate lymphoid cells and asthma. J. Allergy Clin. Immunol. *133*, 943–950, quiz 51.

Yu, G., Wang, L.G., Yan, G.R., and He, Q.Y. (2015). DOSE: an R/Bioconductor package for disease ontology semantic and enrichment analysis. Bioinformatics *31*, 608–609.

Zhang, Y., Liu, T., Meyer, C.A., Eeckhoute, J., Johnson, D.S., Bernstein, B.E., Nusbaum, C., Myers, R.M., Brown, M., Li, W., and Liu, X.S. (2008). Model-based analysis of ChIP-Seq (MACS). Genome Biol. *9*, R137.

STAR★METHODS

KEY RESOURCES TABLE

REAGENT or RESOURCE	SOURCE	IDENTIFIER
Antibodies		
Anti-mouse CD3ε PE/Cy7 (clone 145-2C11)	BioLegend	Cat# 100320
Anti-mouse CD3ε BV421 (clone 145-2C11)	BioLegend	Cat# 100341
Anti-mouse CD4 FITC (clone RM4-5)	BioLegend	Cat# 100510
Anti-mouse CD4 BV421 (clone RM4-5)	BioLegend	Cat# 100544
Anti-mouse CD8α BV421 (clone 53-6.7)	BioLegend	Cat# 100738
Anti-mouse CD11b APC (clone M1/70)	BioLegend	Cat# 101212
Anti-mouse/human CD11b BV421 (clone M1/70)	BioLegend	Cat# 101236
Anti-mouse CD11c PerCP (clone N418)	BioLegend	Cat# 117326
Anti-mouse Cd11c APC (clone N418)	BioLegend	Cat# 117310
Anti-mouse CD11c PE/Cy7 (clone N418)	BioLegend	Cat# 117318
Anti-mouse CD11c BV421 (clone N418)	BioLegend	Cat# 117330
Anti-mouse CD19 APC (clone 6D5)	BioLegend	Cat# 115512
Anti-mouse CD19 BV421 (clone 6D5)	BioLegend	Cat# 115538
Anti-mouse CD45 APC/Cy7 (clone 30-F11)	BioLegend	Cat# 103116
Anti-mouse CD90.2 FITC (clone 30-H12)	BioLegend	Cat# 105306
Anti-mouse CD127 PE (clone A7R34)	BioLegend	Cat# 135010
Anti-mouse CD127 PE/Cy7 (clone A7R34)	BioLegend	Cat# 135014
Anti-mouse/human IL-5 APC (clone TRFK5)	BioLegend	Cat# 504306
Anti-mouse IL-13 PE (clone eBio13A)	Thermo Fisher Scientific	Cat# 12-7133-82
Anti-mouse IL-33Rα PE (clone DIH9)	BioLegend	Cat# 145304
Anti-mouse/rat Ki-67 PE/Cy7 (SolA15)	Thermo Fisher Scientific	Cat# 25-5698-82
Anti-mouse/human KLRG1 APC/Cy7 (clone 2F1/KLRG1)	BioLegend	Cat# 138426
Anti-mouse NK-1.1 APC (clone PK136)	BioLegend	Cat# 108710
Anti-mouse NK-1.1 BV421 (clone PK136)	BioLegend	Cat# 108732
Anti-mouse Siglec-F PE (clone E50-2440)	BD Biosciences	Cat# 552126
Anti-mouse TCRβ PE/Cy7 (clone H57-597)	BioLegend	Cat# 109222
Anti-mouse TCRβ BV421 (clone H57-597)	BioLegend	Cat# 109230
Anti-mouse TCRγ/δ PE/Cy7 (clone GL3)	BioLegend	Cat# 118124
Anti-mouse TCRγ/δ BV421 (clone GL3)	BioLegend	Cat# 118120
Chemicals, Peptides, and Recombinant Proteins		
Recombinant mouse IL-7	BioLegend	Cat# 577802
Recombinant mouse IL-17E	R&D Systems	Cat# 1399-IL-025
Recombinant mouse IL-33	BioLegend	Cat# 580504
CGRP (rat, mouse)	Phoenix Pharmaceuticals	Cat# 015-09
Neuromedin U	US Biological Life Sciences	Cat# N2171-80E
Dibutyryl-cAMP	Tocris	Cat# 1141
7AAD	BD Biosciences	Cat# 559925
Fixable Viability Dye eFluor 506	Invitrogen	Cat# 65-0866-14
Critical Commercial Assays		
Lung Dissociation Kit, mouse	Miltenyi Biotec	Cat# 130-095-927
gentleMACS C tubes	Miltenyi Biotec	Cat# 130-096-334
CD90.2 MicroBeads, mouse	Miltenyi Biotec	Cat# 130-049-101
LegendPlex (Mouse Th Cytokine Panel)	BioLegend	Cat# 740005

(*Continued on next page*)

Continued

REAGENT or RESOURCE	SOURCE	IDENTIFIER
LegendPlex (Mouse Th2 Cytokine Panel)	BioLegend	Cat# 740027
CellTrace Violet Cell Proliferation Kit	Invitrogen	Cat# C34557
BD Cytofix/Cytoperm	BD Biosciences	Cat# 51-2090KZ
BD Perm/Wash	BD Biosciences	Cat# 51-2091KZ
Fixation/Permeabilization Concentrate	Invitrogen	Cat# 00-5123-43
Fixation/Perm Diluent	Invitrogen	Cat# 00-5223-56
Permeabilization Buffer	Invitrogen	Cat# 00-8333-56
RNeasy Plus Mini Kit	QIAGEN	Cat# 74134
PicoPure RNA Isolation Kit	Thermo Fisher Scientific	Cat# KIT0204
RNase-Free DNase Set	QIAGEN	Cat# 79254
iScript cDNA Synthesis Kit	Bio-Rad	Cat# 1708891
SuperScript IV VILO Master Mix	Thermo Fisher Scientific	Cat# 11756050
TaqMan Fast Advanced Master Mix	Thermo Fisher Scientific	Cat# 4444557
Nextera DNA Preparation Kit	Illumina	Cat# FC-121-1031
Chromium Single Cell 3′ GEM, Library & Gel Bead Kit v3	10x Genomics	Cat# 1000075
HiSeq X Ten Reagent Kit v2.5	Illumina	Cat# FC-501-2501
Deposited Data		
Raw and analyzed data	This paper	GEO: GSE136154
ScRNA-seq samples (related to Figure S1 and Figure 2)	Wallrapp et al., 2017	GEO: GSE102299
Experimental Models: Organisms/Strains		
Mouse: C57BL/6J	The Jackson Laboratory	JAX: 000664
Mouse: Rag2−/− mice	The Jackson Laboratory	JAX: 008449
Mouse: CGRP-GFP	McCoy et al., 2012	N/A
Mouse: Foxp3-GFP	Bettelli et al., 2006	N/A
Mouse: CGRP−/−	Oh-hashi et al., 2001	N/A
Mouse: Ramp1−/−	Tsujikawa et al., 2007	N/A
Software and Algorithms		
FlowJo v10.5.0	FlowJo	www.flowjo.com
Prism v7.0a and v8.1.2	GraphPad	www.graphpad.com
R v3.4.1 and v3.5.3	R	www.r-project.org
RStudio v1.0.153 and v1.2.1335	RStudio	www.rstudio.com
DESeq2 version 1.24.0	Love et al., 2014	https://bioconductor.org/packages/release/bioc/html/DESeq2.html
MACS2 version 2.1.1	Zhang et al., 2008	https://pypi.org/project/MACS2/
Bedtools version 2.26.0	Quinlan and Hall, 2010	https://bedtools.readthedocs.io/en/latest/content/history.html
GREAT version 3.0.0	McLean et al., 2010	http://great.stanford.edu/public/html/
The Integrative Genomics Viewer (IGV)	Robinson et al., 2017	http://software.broadinstitute.org/software/igv/

LEAD CONTACT AND MATERIALS AVAILABILITY

Further information and requests for resources and reagents should be directed to and will be fulfilled by the Lead Contact, Vijay K. Kuchroo (vkuchroo@evergrande.hms.harvard.edu).

EXPERIMENTAL MODEL AND SUBJECT DETAILS

Animals

All experiments involving mice were approved by the Institutional Animal Care and Use Committee (IACUC) at Brigham and Women's Hospital. Mice were maintained in the animal facility at Brigham and Women's Hospital under specific pathogen-free conditions with food and water *ad libitum* and a 12 h dark/light cycle. Mice were age- and sex-matched for experiments and were randomly assigned

to experimental groups. C57BL/6J (WT) mice and *Rag2*$^{-/-}$ mice were purchased from the Jackson Laboratory. CGRP-GFP mice (McCoy et al., 2012) were provided by I. Chiu (Harvard Medical School, Boston). FoxP3-GFP mice (Bettelli et al., 2006) were generated in our laboratory. *Calca*$^{-/-}$ mice (Oh-hashi et al., 2001) were provided by Hiroki Kurihara (The University of Tokyo, Tokyo) and distributed by RIKEN BioResource Research Center. *Ramp1*$^{-/-}$ mice (Tsujikawa et al., 2007) were provided by Wade Kingery (Veterans Affairs Palo Alto Health Care System) with permission by Kazutake Tsujikawa (Osaka University, Osaka).

Primary Cell Culture

Primary cells were cultured in a humidified incubator at 37°C and 10% CO2 in complete medium consisting of RPMI 1640 medium (Cat# 11875-119; Thermo Fisher Scientific) supplemented with 10% fetal bovine serum, HEPES, L-Glutamine, Penicillin/Streptomycin and β-Mercaptoethanol.

METHOD DETAILS

Isolation of lung cells for fluorescence-activated cell sorting

Mice were euthanized and perfused with 8ml cold DPBS via the right heart ventricle. Lung lobes were removed from the chest cavity and transferred into gentleMACS C tubes containing Buffer S and enzymes A and D from the lung dissociation kit (Cat# 130-095-927; Miltenyi Biotec). After manual dissociation of the tissue by running program lung_01 of the automated tissue dissociator (gentleMACS; Miltenyi Biotec), and digestion at 37°C for 25min on a rotator, the tissue pieces were further dissociated by running program lung_02 of the automated tissue dissociator. Subsequently, the single-cell suspension was passed through a 70μm cell strainer and washed with DPBS (Cat# 14190-144; Thermo Fisher Scientific) containing 0.5% bovine serum albumin (Cat# BP1600-1; Fisher Scientific) and 2mM EDTA. After incubation of the cells with CD90.2 MicroBeads (Cat# 130-049-101; Miltenyi Biotec) on ice for 17min, cells were washed and transferred onto LS columns (Cat# 130-042-401; Miltenyi Biotec) to enrich for CD90.2-positive cells by positive selection. Then, positive and negative cell fractions were stained with surface antibodies for 20min on ice in the dark, washed and resuspended in 1-2ml DPBS containing 0.5% bovine serum albumin and 2mM EDTA. Cells were purified by fluorescence-activated cell sorting using a BD FACS Aria IIIu flow cytometer with 3 lasers (405nm, 488nm, 640nm) or 4 lasers (405nm, 488nm, 561nm and 640nm) (BD Biosciences). For subsequent cell culture, cells were sorted into complete medium. For RNA isolation, cells were directly sorted into RLT Plus lysis buffer (RNeasy Plus Mini Kit; QIAGEN) or extraction buffer (PicoPure RNA Isolation Kit; Thermo Fisher Scientific). Debris and doublets were excluded for cell types using forward and sideward scatter. The CD90.2 positive cell fraction was used to sort innate lymphoid cells (ILCs) (7AAD-, CD45+, CD90.2+, Lineage (CD3, CD4, CD8, CD11b, CD11c, CD19, NK1.1, TCRβ, TCRγδ)-, CD127+ cells), ILC2s (ST2+ ILCs), CD4 T cells (7AAD-, CD45+, CD3+, CD4+, TCRβ+ cells) and TCRγδ T cells (7AAD-, CD45+, CD3+, CD4-, TCRβ-, TCRγδ+). The CD90.2 negative fraction was used to sort B cells (7AAD-, CD45+, CD19+), eosinophils (7AAD-, CD45+, CD11b+, CD11c$^{-/low}$, Siglec-F+, SSC-A^{hi}), neutrophils (7AAD-, CD45+, CD11b+, CD11c^{-}, Siglec-F-, Ly6G+), macrophages (7AAD-, CD45+, CD11b+, CD11c+, F4/80+, Siglec-F+, MHC2+) and CD45- cells (7AAD-, CD45-). For the isolation of inflammatory ILC2s, single-cell suspension was enriched for lymphocytes by 40/70% Percoll gradient centrifugation instead of enrichment with CD90.2 beads. Inflammatory ILC2s were defined as 7AAD-, CD45+, CD127+, Lineage-, CD90.2^{int}, ST2-, KLRG1+ cells and gated as shown in Figure S3.

Culture of innate lymphoid cells

Sort-purified innate lymphoid cells (ILCs) were cultured under sterile conditions in complete medium in a humidified incubator at 37°C and 10% CO2. ILCs were plated at a density of 3,000-5,000 ILCs per well in a 96 well round-bottom plate in complete medium with 20ng/mL IL-7. Depending on the experiment, different combinations of 200ng/mL IL-25, 200ng/mL IL-33, 1μg/mL NMU, 100nM CGRP or 100μM dibutyryl-cAMP were added either at start or after overnight culture with 20ng/mL IL-7. After 6 h or 3 days, culture supernatant was removed and frozen at −20°C and ILCs were lysed in Extraction Buffer (PicoPure RNA isolation Kit; Thermo Fisher Scientific), incubated at 42°C for 30min and frozen at −80°C.

Proliferation assay

Lung cells were isolated and enriched for CD90.2 cells as described above, followed by labeling with CellTrace Violet (Cat# C34557; Thermo Fisher Scientific) according to manufacturer's instructions and subsequently stained with antibodies. After 3-day culture of sort-purified ILCs with 20ng/mL IL-7 either alone or in combination with 200ng/mL IL-33, 100pM CGRP or 100nM CGRP followed by staining, expression of CellTrace Violet in live (7AAD-) ILCs was analyzed on a BD LSRFortessa (BD Biosciences).

Airway inflammation

Mice received nasally 500ng IL-25, 500ng IL-33, 20μg NMU, 6.65μg CGRP or 50μg papain diluted in DPBS for three consecutive days. For nasal administration, mice were lightly anesthetized with Isoflurane (Cat# 07-893-1389; Patterson Veterinary). For induction of inflammatory ILC2s, mice received intraperitoneally 500ng IL-25 for three consecutive days. One day after the last treatment, mice were euthanized and perfused with 8ml cold DPBS via the right heart ventricle. After exposure of the trachea, a small incision was made at the top of the trachea and a curved gavage needle was inserted. Lungs were washed with 1.5ml cold DPBS via the needle and the retrieved bronchoalveolar lavage fluid was centrifuged at 1300rpm for 5 min at 4°C. After centrifugation, the supernatant was frozen at −20°C and the cell pellet was resuspended in 250μl complete medium and stored on ice until flow cytometric analysis. The

post-caval lung lobe was transferred into 10% buffered formalin and stored at room temperature until paraffin embedding for histological analysis. The other lung lobes were dissociated using the lung dissociation kit (Cat# 130-095-927; Miltenyi Biotec) and automated tissue dissociator (gentleMACS; Miltenyi Biotec) as described above with the adjustment that after running program lung_02, the single cell suspension was centrifuged at 1300rpm for 5 min at 4°C and 1ml of the supernatant was frozen at −20°C. Single-cell suspension was resuspended in complete cell culture medium and stored on ice until further processing.

For RNA isolation, lung cells were centrifuged at 300 g for 6 min at 4°C, the supernatant was discarded and the cell pellet was resuspended in 600μl RLT Buffer Plus (QIAGEN RNA isolation kit), vortexed and frozen at −80°C.

For cell counts, lung cells were stained with 7AAD and Precision Count Beads (Cat# 424902; BioLegend) were added according to manufacturer's instructions. Cells and beads were acquired on a BD LSRFortessa (BD Biosciences) and cell numbers were calculated based on number of acquired live (7AAD-) cells and number of acquired beads.

For flow cytometric analysis, lung cells were transferred into a 96 well V-bottom plate and stained with surface antibodies for 20min at 4°C in the dark. Cells were washed twice with DPBS containing 2% fetal bovine serum and transferred into 1.2ml tubes for analysis by flow cytometry. For intracellular cytokine staining, cells were incubated in complete cell culture medium with 50ng/mL phorbol 12-myristate 13-acetate (Sigma-Aldrich), 1μM ionomycin (Sigma-Aldrich) and GolgiStop (Cat# 554724; BD Biosciences) for 5 h and fixed and stained using the BD Fixation/Permeabilization Solution Kit (Cat# 554714; BD Biosciences) per manufacturer's instructions. For ki67 staining, cells were fixed with the Foxp3/Transcription Factor Staining Buffer Set (Cat# 00-5223-00; Invitrogen) per manufacturer's instructions. Cells were analyzed on a BD LSRFortessa (BD Biosciences) flow cytometer with 5 lasers (355nm, 405nm, 488nm, 561nm and 640nm). Data was analyzed using FlowJo v10.5.0 software and cell populations were gated as described previously (Wallrapp et al., 2017).

RNA isolation and cDNA synthesis

RNA was isolated from lung cells and immune cell populations sorted from naive mice using the QIAGEN RNeasy Plus Mini Kit (Cat# 74134; QIAGEN) according to manufacturer's instructions. RNA concentration and purity were determined with a NanoDrop spectrophotometer (Thermo Fisher Scientific) and equal amounts of RNA were reverse transcribed to cDNA using the iScript cDNA Synthesis Kit (Cat# 1708891; Bio-Rad). RNA was isolated from cultured ILCs or *ex vivo* sort-purified ILCs with the PicoPure RNA isolation kit (Cat# KIT0204; Thermo Fisher Scientific) according to manufacturer's instructions and subsequently reverse transcribed to cDNA with the SuperScript IV VILO Master Mix (Cat# 11756050; Thermo Fisher Scientific). To analyze gene expression TaqMan Fast Advanced Master Mix (Cat# 4444557; Thermo Fisher Scientific) was used per manufacturer's directions and quantitative real-time PCR was performed with a ViiA 7 system (Thermo Fisher Scientific). Gene expression was normalized to expression of the housekeeping gene Actin-b. The following TaqMan probes were used: *Il5* (Mm00439646_m1), *Il13* (Mm00434204_m1), *Ramp1* (Mm00489796_m1), *Ramp3* (Mm00840142_m1), *Calcrl* (Mm00516986_m1), *Calca* (Mm01274759_g1), *Areg* (Mm00437583_m1), *Foxp3* (Mm00475162_m1) and *Actb* (Cat#4352341E; Thermo Fisher Scientific).

Bead-based immunoassay

Cytokine concentrations in bronchoalveolar lavage fluid, lung tissue and ILC culture supernatant were determined using the LEGENDplex mouse Th cytokine panel (Cat# 740005; BioLegend) or mouse Th2 cytokine panel (Cat# 740027; BioLegend) according to manufacturer's instructions. Samples were acquired using a BD LSRFortessa flow cytometer (BD Biosciences) and analyzed with the LEGENDplex Software v7.1.

Methacholine assay

Mice were anesthetized and a 20G needle was inserted into the trachea and connected to a flexiVent FX1 instrument (SCIREQ). Mice were exposed to increasing doses of aerosolized methacholine (0, 3, 10, 30, 100mg/mL diluted in DPBS) and airway resistance was measured. For each dose the airway resistance was calculated as the mean of 8 measurements.

Histology

Lung tissue was fixed in 10% buffered formalin at room temperature and embedded in paraffin. After sectioning, lung slices were stained with hematoxylin and eosin (H&E) and scored for severity of airway inflammation by a histopathologist in a blinded manner according to the following scoring system: 0, normal; 1, very mild; 2, mild; 3, moderate; 4, severe.

ATAC-seq

ILC2s were cultured as described above for 6 h with IL-33 or IL-33+CGRP. Subsequently, 6,000 viable ILC2s were sorted into DPBS supplemented with 2% FCS. Cells were pelleted by centrifugation and stored in Bambanker™ cell freezing media (LYMPHOTEC Inc.) at −80°C. For ATAC-seq library preparation, cells were thawed at 37°C, washed once with PBS, and lysed and tagmented in 1X TD Buffer, 0.2μl TDE1 (Illumina), 0.01% digitonin, and 0.3X PBS in 40μl reaction volume following the protocol described in *Corces at al.* (Corces et al., 2016). Transposition was performed at 37°C for 30 min at 300 rpm. The DNA was purified immediately with the MinElute PCR purification kit (QIAGEN). The complete eluate was then amplified with PCR, as follows. First, 5 cycles of pre-amplification were performed using indexed primers with NEBNext High-Fidelity 2X PCR Master Mix (NEB). The number of additional cycles was assessed by SYBR Green quantitative PCR. After purifying the final library with the MinElute PCR purification kit (QIAGEN), the library

was quantified with the Kapa Library Quantification Kit (Kapa Biosystems) and a Qubit dsDNA HS Assay kit (Invitrogen). Libraries were sequenced on an Illumina NextSeq 550 system with paired-end reads of 37 base pairs in length.

ATAC-seq data processing

Read alignment, filtering, visualization of signal tracks, and measurement of quality control metrics was performed using a publicly available ATAC-seq pipeline (Lee et al., 2016). Briefly, reads were aligned to the mm10 genome using Bowtie2 and filtered to remove duplicates and mitochondrial reads. Alignment files were merged for biological replicates for peak-calling using MACS2 (Zhang et al., 2008). Read counts per peak were compiled using the bedtools multicov tool. Counts were normalized and processed for differential peak accessibility between conditions using DESeq2 (Love et al., 2014). Gene annotation with putative regulatory elements was performed using GREAT with default parameters (McLean et al., 2010). Briefly, genes were assigned a minimum basal regulatory domain from −5 kb to +1 kb from the transcription start site and extending up to the nearest gene's basal regulatory domain. ATAC-seq peaks were assigned to any gene with an intersecting regulatory domain as a potential regulatory element of that gene (Table S3).

Previously published single-cell RNA-Seq data

Processed scRNA-Seq data was obtained from our earlier study (Wallrapp et al., 2017), without any change to processing, using the same expression values and cluster assignments as previously reported. In particular, log-transformed normalized gene expression levels, referred to as log TPX, were calculated by calling Seurat's LogNormalize() function with the scale set to reflect the expected number of UMIs in each condition. That is, for cells in condition c and batch i to, the "scale.factor" argument was set to 10, 000 × $(w_{c,i}/\text{mean}_i(w_{PBS,i}))$, where $w_{c,i}$ is the mean number of UMIs per cell in condition c and batch i (Wallrapp et al., 2017).

Bulk RNA-seq

ILCs were plated in replicates and cultured as described above for 3 days and RNA was isolated using PicoPure RNA isolation kit according to manufacturer's instructions. Two replicates from each of two distinct experiments were subsequently sequenced. RNA was quantified using a Qubit RNA HS Assay kit (Invitrogen) and quality accessed with a RNA 6000 Pico Kit (Agilent). 2ng of RNA were used as input for a modified SMART-Seq2 protocol (Picelli et al., 2014) entailing RNA secondary structure denaturation (72°C for three minutes), reverse transcription with Maxima Reverse Transcriptase (Life Technologies), and whole transcriptome amplification (WTA) with KAPA HiFi HotStart ReadyMix 2X (Kapa Biosystems) for 12 cycles. WTA products were purified with Ampure XP beads (Beckman Coulter), quantified with a Qubit dsDNA HS Assay Kit (Invitrogen), and quality assessed with a High Sensitivity DNA Chip run on a Bioanalyzer 2100 system (Agilent). 0.2 ng of purified WTA product was used as input for Nextera XT DNA Library Preparation Kit (Illumina). Uniquely barcoded libraries were pooled and sequenced with a NextSeq 500 sequencer using a high output V2 75 cycle kit (Illumina) and 2x38 paired end reads.

Bulk RNA-seq data processing

Raw data was converted to fastq files using bcl2fastq 2.17.1.14 with options "–minimum-trimmed-read-length 10–mask-short-adapter-reads 10." Transcript quantification was done using Kallisto 0.42.3 (Bray et al., 2016) with the mm10 mouse genome annotation, and transcript counts were then converted to gene counts and normalized TPM values using the R package tximport (Soneson et al., 2015).

Bulk RNA-seq analysis

Differential expression was analyzed using the DESeq2 R package (Love et al., 2014). At each time point, gene expression was modeled as a sum of the effects of the condition and of the batch, i.e., date of the experiment. For the joint analysis of both time points, gene expression was modeled as a sum of the effects of the condition, batch, and time point, with an interaction term for condition and time point. For the IL-33+CGRP condition, the null condition was IL-33 treatment. For the IL-7+CGRP condition, which was analyzed separately, the null condition was IL-7 treatment. Significance of the overall model fit was estimated by a likelihood ratio test (LRT), where the reduced model consisted of only the batch variable. P values were automatically adjusted by DESeq2 using independent filtering for an FDR of 0.1. Genes that had an adjusted p value for the LRT of at most 0.05 ("LRT-filtered") are included on the sheets of Table S2. LRT-filtered genes were considered *significantly differentially expressed* if, in addition, they met the criteria of having a Wald test adjusted p value for the condition variable of at most 0.05, and absolute value of the associated log fold change of at least log2(1.5). Tests of enrichment in gene sets from GO (Table S4) and other sources were performed on these genes and visualized using the R packages clusterProfiler (Yu et al., 2012) and DOSE (Yu et al., 2015). The negative regulatory gene set used in comparisons consists of the cell surface transmembrane receptors *Ctla4, Havcr2, Icos, Lag3, Lilrb4, Pdcd1, Tigit, Tnfrsf4, Tnfrsf9,* and *Tnfrsf18* (Chihara et al., 2018).

CGRP response gene signature derivation

The CGRP signature was defined as the set of genes that satisfy all the following criteria: (1) LRT-filtered in the 3-day CGRP+IL-33 versus IL-33 model and CGRP+IL-7 versus IL-7 model; (2) significantly differentially expressed at least in one of those models; (3) having model coefficients of the same sign in each comparison, i.e., corresponding to fold changes in the same direction in both models. The sign of the gene in the CGRP signature corresponded to the sign of the coefficient in the models (Table S5).

Gene signature scoring and analysis

A score for an individual cell in the single-cell RNA-seq dataset was calculated as the log of the geometric mean of the normalized expression (TPX) values of the genes in the signature. Genes with a negative sign in the signature contributed negatively to the score, and genes that did not appear in the single-cell dataset but appeared in the signature contributed as zero values. Using linear regression, the signature score was modeled as a sum of the effects of the cluster (or the condition) and the log of the number of UMIs. Cluster 9 in the previously published scRNA-seq data had statistically significantly higher CGRP signature scores, regardless which other cluster was used as the reference.

New single-cell RNA-seq

Library preparation

Lung ILCs were sorted from mice, which had received nasally PBS, CGRP, IL-33 or IL-33+CGRP for 3 consecutive days, into DPBS with 0.4% BSA. Subsequently, cells were encapsulated into droplets and libraries were prepared using the Chromium Single Cell 3′ GEM, Library & Gel Bead Kit v3 (10x Genomics) per manufacturer's instructions. Generated libraries were sequenced on a HiSeq X (Illumina).

Initial data processing and QC

Gene counts were obtained by aligning reads to the mm10 genome using CellRanger software (v1.3) (10x Genomics). To remove doublets and poor-quality cells, cells were excluded from subsequent analysis if they were outliers in their sample or condition of origin in terms of number of genes or number of unique molecular identifiers (UMIs), which left 83.1% and 84.2% of cells from CGRP and PBS, respectively, and 90.3% and 93% of cells from IL-33 and IL-33+CGRP conditions, respectively (Figure S7A). Sample-specific cut-offs per cell were 900–5,000 genes for IL-33 and IL-33+CGRP conditions and 900–3,900 genes for CGRP and PBS. Another 2.1% of the remaining cells were excluded for having greater than 10% of mitochondrial gene counts (Figures S7B and S7C).

Normalization and Dimensionality Reduction

To normalize gene counts, we used regularized negative binomial regression via the SCTransform() function from Seurat v3, with the ''batch_var'' parameter set to the replicate indicator variable and the ''vars_to_regress'' parameter set to the variable capturing the percentage of mitochondrial gene counts in each cell (Butler et al., 2018; Hafemeister and Satija, 2019). This step takes the place of the typical steps of log-normalization, variable gene selection, and scaling. We used log1p of the corrected counts to compute principle components analysis (PCA), and used the top 40 PCs as input to the visualization embedding by uniform manifold approximation and projection (UMAP).

Clustering and Differential Expression

The processed data was imported into SCANPY (v1.4), where the neighborhood graph was computed using 15 neighbors and 20 PCs (Wolf et al., 2018). Clustering was done using the Leiden algorithm with a resolution of 0.6. Differentially expressed genes were computed using the default settings of the sc.tl.rank_genes_groups() function, which uses 't test_overestim_var' as the method and uses for comparison all cells outside of the group (e.g., cluster or condition) of interest (Table S6). Logistic regression analyses used generalized linear regression with batch and log of the number of UMIs as nuisance variables.

QUANTIFICATION AND STATISTICAL ANALYSIS

Statistical analysis was performed with GraphPad Prism software version 7.0a and 8.1.2 (GraphPad). Data are shown as mean ± SEM. Statistical significance was determined using unpaired two-tailed t test (when comparing two groups) or a one-way ANOVA with Tukey's multiple comparisons test (for the comparison of three or more groups) unless otherwise indicated.

DATA AND CODE AVAILABILITY

Code will be made available at https://github.com/sriesenfeld/CGRP_LungILCs_Analyses. The accession number for the ATAC- and RNA-seq data reported in this paper is NCBI Gene Expression Omnibus: GSE136154.